Zebrafish as research model to study Gaucher disease: Insights into molecular mechanisms

Lelieveld, L.T.

CHAPTER 7

Progression of pathology in zebrafish with GCase deficiency

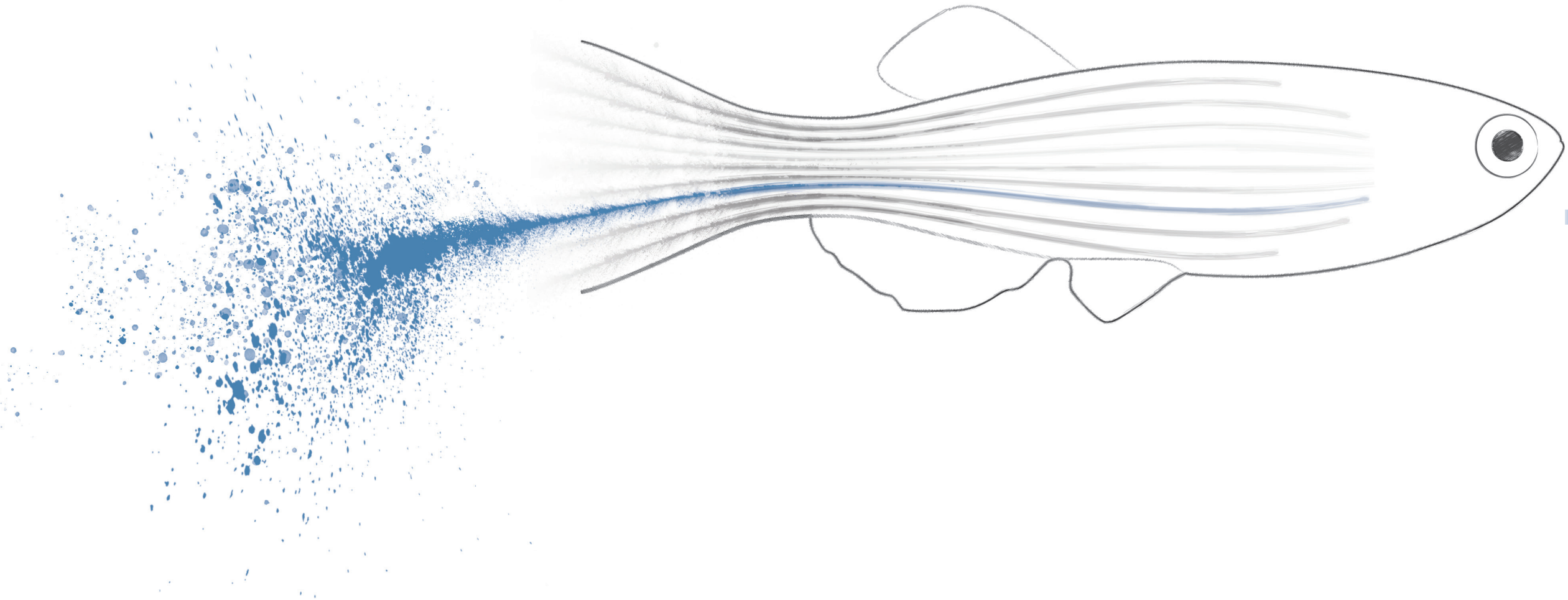

Abstract

The penultimate step in the degradation of glycosphingolipids is the hydrolysis of glucosylceramide into glucose and ceramide. GlcCer is degraded in lysosomes by the acid β-glucosidase glucocerebrosidase (GCase). Mutations in the gene encoding GCase (gene name: *GBA*) lead to the common lysosomal storage disorder Gaucher disease (GD), characterized by lysosomal accumulation of GlcCer which partly is metabolized by acid ceramidase (ACase) into neurotoxic glucosylsphingosine (GlcSph). GlcCer can also be hydrolysed in the cytosol by the membrane-associated GBA2. Defective GBA2 has been found in association with autosomal-recessive cerebellar ataxia (ARCA) and hereditary spastic paraplegia (HSP). In the present study, zebrafish with complete knockouts (KOs) of the genes encoding GCase (*gba1)*, Gba2 (*gba2*), ACase (*asah1b*) and combinations thereof, were raised to adulthood (12 weeks post-fertilization (wpf)) and characterized. Their phenotype as well as biochemical and pathological parameters are described. Carrier *gba1*$^{+/-}$ fish show no apparent phenotype nor any biochemical abnormalities, while the Gba2 knockout fish only develop a significant increase in specific GlcCer species in the brain. No clear abnormal phenotype is observed for any of the GCase deficient fish at 8 wpf, even though increases in GlcCer, neuroinflammation and autophagy are already demonstrable. Phenotypic abnormalities of the single *gba1* knockout zebrafish have an early onset (± 9 wpf), starting with a drop of the tail and progressing into a change in swimming behaviour. In contrast, the double *gba1:gba2* knockout do not show the preceding characteristics such as the drop of the tail, but many develop a severe phenotypical abnormalities in a matter of days and have a significantly shorter lifespan than single *gba1* knockouts. Pilot experiments indicate a related earlier onset of dopaminergic neuron degradation in the *gba1:gba2* knockout fish, however the precise underlying pathophysiological mechanism is still elusive.

Introduction

Glucosylceramide (GlcCer) is the precursor of more complex glycosphingolipids. Hydrolysis of GlcCer into glucose and ceramide is catalysed by different β-glucosidases with different subcellular locations (**Figure 1**). Acid β-glucosidase, or glucocerebrosidase (GCase), is a lysosomal β-glucosidase, hydrolysing GlcCer in lysosomes, while the membrane-associated GBA2 and cytosolic GBA3 hydrolyse GlcCer in the cytosol. Mutations in the gene encoding GCase lead to Gaucher disease, characterized by lysosomal accumulation of GlcCer primarily in tissue macrophages[1]. Clinical symptoms range from hepatosplenomegaly, anaemia, thrombocytopenia to bone deterioration in type 1 GD patients and, additionally, neuropathological symptoms in type 2 and 3 GD patients. Lysosomal acid ceramidase (ACase) is able to hydrolyse the fatty acid of the accumulating GlcCer, forming glucosylsphingosine (GlcSph). GlcSph is thought to be neurotoxic and to contribute to B-cell activation, α-synuclein aggregation and reduced cerebral microvasculature[2-5]. Carriers of a mutation in GCase, have a markedly increased risk for developing Parkinson's disease and Lewy-body dementia[6,7]. However, to date, the underlying molecular mechanisms, imposed by GCase abnormalities, are not fully elucidated. Little is known about the physiological role of the non-lysosomal GBA2 and the impact of its deficiency. On one hand, mutations in the gene encoding GBA2 have been associated with autosomal-recessive cerebellar ataxia (ARCA) and hereditary spastic paraplegia (HSP)[8-11]. On the other hand, mildly affected type 1 GD patients are treated for more than a decade with the iminosugar Miglustat (*N*-butyl-deoxynojirimycin) and develop no major complications, even though this compound markedly inhibits GBA2 activity at the administered dose (3 times 100 mg daily)[12,13].

In the past years, several research models have been generated in order to study the impact of defective GCase or GBA2 and evaluate treatments of GD[14]. Complete GCase-deficient mouse models die prematurely due to trans-epidermal water loss[15,16]. For that reason, GD has been studied by pharmacological induction of GCase deficiency[17] or using conditional knockouts of *GBA1* where GCase deficiency is limited to specific cell lineages. Examples are the GD mouse models with a defective GCase in the hematopoietic stem cell lineage[18], neuronal cells[19] or all tissues except skin[19]. GBA2 knockout mice are viable and develop a moderately increased GlcCer in testis, brain and liver (Marques and Ferraz; unpublished data and ref. 20). Male KO mice are found to display impaired fertility[20-22]. Remarkable interindividual differences were recently noted among GBA2 deficient mice with some animals developing marked neurological abnormalities and others not[21]. Interestingly, concomitant GBA2 deficiency in a conditional GCase deficient mouse model, limited to the haematopoietic stem cell lineage, revealed a correction of the visceral, hematologic and bone phenotype. In addition, a partial correction of increased cytokines was observed, even though persistent Gaucher cells were observed as well as increased GlcCer and GlcSph levels in liver and spleen of double mutant mice[23]. Amelioration of phenotypic manifestations of Niemann-Pick type C (NPC) mice, including behaviour and neuropathology, were apparent in mice with a concomitant genetic- or pharmacological GBA2 deficiency upon treatment with GBA2-specific iminosugars[24]. At present the impact of defective GBA2 in GD mice regarding neurological symptoms remains elusive.

Recent research has revealed that both GCase and GBA2 have substrates beyond GlcCer. Both enzymes may act as transglucosidase, catalysing the (reversible) transfer of the glucose from GlcCer to an acceptor moiety such as cholesterol and thereby forming glucosylated cholesterol (GlcChol, **Figure 1**)[25,26]. GD patients and GD mouse models show an increase in GlcChol levels, while GBA2 deficient mice show a decrease[25]. Although GCase can perform transglucosylation *in vitro*, increased levels of GlcChol during GCase deficiency suggest a primary role of the enzyme in hydrolysis of lysosomal GlcChol[25]. It is presently unclear whether elevated GlcChol during GCase deficiency contributes to pathology. Previously, CRISPR/Cas9 technology was successfully used to generate mutations in the zebrafish orthologues of GCase and GBA2. The developing zebrafish off-spring of 5 days post-fertilization (5 dpf) were studied regarding aberrant glucosylceramide metabolism of *gba1*, *gba2* and double *gba1:gba2* knockout (KO) individuals. At 5dpf, single *gba1*$^{-/-}$ zebrafish larvae show accumulation of GlcSph, but no GlcCer accumulation, while single *gba2*$^{-/-}$ zebrafish larvae show accumulation of GlcCer and a decrease in GlcChol[27].

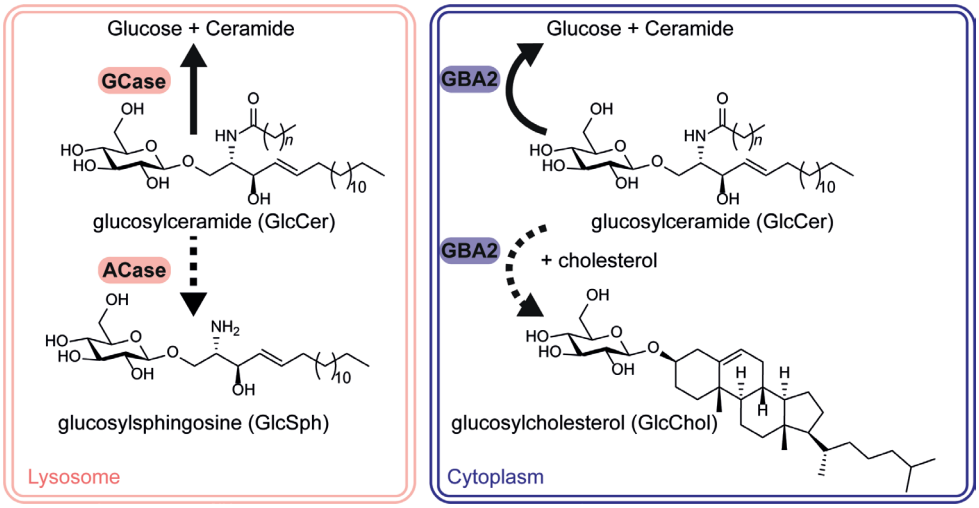

Figure 1 | Schematic representation of GlcCer hydrolysis by lysosomal GCase and membrane-associated GBA2. Secondary pathways of GlcCer catabolism are described. ACase is able to hydrolyse accumulating lysosomal GlcCer to GlcSph during GCase deficiency. Next to hydrolysis of GlcCer, GBA2 is also able to transfer the glucose of GlcCer to a cholesterol acceptor, generating GlcChol.

The primary goal of the present study was to evaluate adult Gba2 KO zebrafish and to study the impact of the absence of Gba2 during GCase deficiency. For this purpose, zebrafish were raised to adulthood and several morphological, histopathological and biochemical features were assessed and compared between the different mutants. This study also included *gba1*$^{+/-}$ (carriers), *asah1b*$^{-/-}$ and *gba1*$^{-/-}$*:asah1b*$^{-/-}$ fish. Given the significant difference in occurrence of symptoms and accompanying lifespan of *gba1*$^{-/-}$, *gba1*$^{-/-}$*:gba2*$^{-/-}$ and *gba1*$^{-/-}$*:asah1b*$^{-/-}$ fish, attention was paid to the progression of pathology in the various mutant zebrafish. Zebrafish with gba*1*, *gba2, gba1:gba2* and *asah1b:gba1* mutations were examined at different developmental ages with respect to neuroinflammation that likely precedes neurodegeneration.

Results

Lipid abnormalities of *gba1:gba2* KO zebrafish as compared to *gba1* and *gba1:asah1b* KO

Glycosphingolipids in brains and livers of 12 wpf zebrafish with a KO of *gba1*, *gba2* and *asah1b* and combinations thereof were quantified. Recently, Hisako Akiyama at the RIKEN discovered the existence of galactosylcholesterol (GalChol) in tisssues, particularly the brain[28]. GalChol is synthesized by GBA2. With the initial LC-MS/MS method GlcChol and GalChol were not separated. This prompted the use of a different LC chromatography in order to individually measure GlcChol and GalChol. With this method in place, brains of mutant zebrafish were investigated. Brains and livers of *gba1*$^{-/-}$ zebrafish presented significantly increased GlcSph, total GlcCer, lactosylceramide (LacCer) and GlcChol levels but no significantly elevated GalChol, ceramide and sphingosine levels (brain) (**Figure 2A** and **B** for liver and brain respectively). A reduction in galactosylceramide (GalCer) levels was apparent in *gba1*$^{-/-}$ but this was not significantly different.

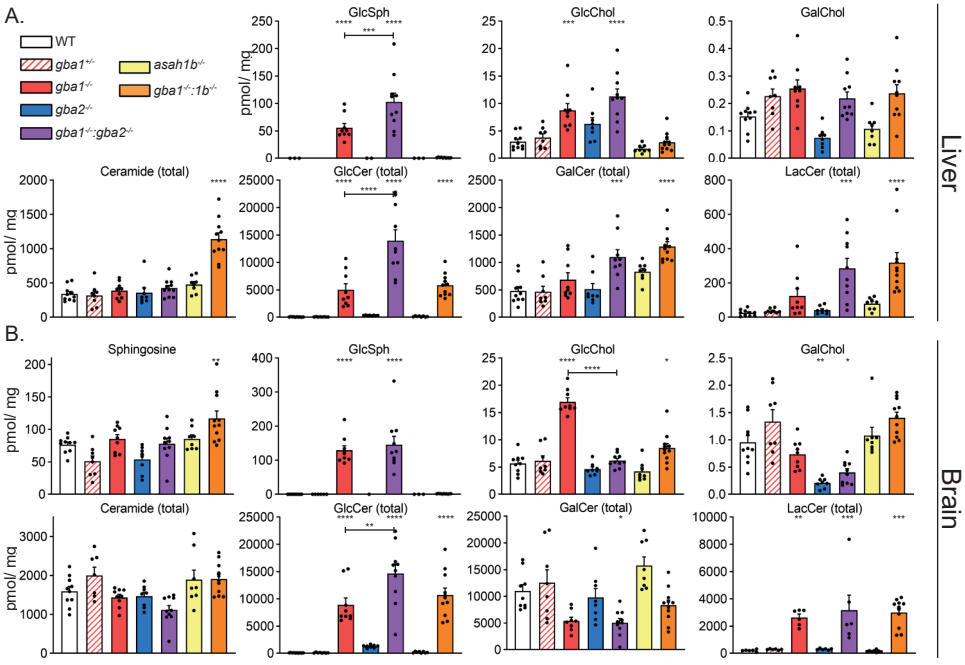

Figure 2 | Relevant (glyco)sphingolipids in livers and brains of end stage zebrafish (t = 9-12 wpf)

Relevant glycosphingolipids, GlcSph, GlcChol, GalChol as well as total ceramide, total GlcCer, total GalCer and total LacCer, were determined of zebrafish livers and brains in pmol/mg tissue. Livers and brains were dissected of zebrafish at t= 12 wpf or at the end stage, following pre-determined human end points for *gba1*$^{-/-}$ (t= 10-12 wpf) and gba1$^{-/-}$:gba2$^{-/-}$ zebrafish (t = 9-12 wpf). Data is depicted as mean ± SEM; end stage; (n = 8-11). Data is analysed by One-Way Anova with Tukey's multiple comparison test. Ns = not significant, ** P < 0.01, *** P < 0.001 and **** P < 0.0001.

Gba1$^{-/-}$*:asah1b*$^{-/-}$ brains and livers displayed no excessive GlcSph, while total GlcCer and LacCer levels were increased (see also chapter 6). No significant accumulation of GlcChol was observed in the *gba1*$^{-/-}$*:asah1b*$^{-/-}$ brains in contrast to the *gba1*$^{-/-}$ brains.

No significant differences were apparent in any of the lipids quantified in brains and livers of *gba1*$^{+/-}$ (carrier) zebrafish compared to wildtype (WT) (striped bars, **Figure 2A** and **B**). GlcSph, total GlcCer and LacCer levels were significantly elevated in the *gba1*$^{-/-}$*:gba2*$^{-/-}$ livers and brains compared to WT (purple bars, **Figure 2A** and **B**). Statistical analysis revealed that GlcCer levels of *gba1*$^{-/-}$*:gba2*$^{-/-}$ livers and brains were significantly higher compared to single *gba1*$^{-/-}$ and *gba1*$^{-/-}$*:asah1b*$^{-/-}$ samples, while only significant higher GlcSph levels were detected in livers of *gba1*$^{-/-}$*:gba2*$^{-/-}$, compared to those of *gba1*$^{-/-}$ fish. GalCer levels were significantly reduced in the double *gba1*$^{-/-}$*:gba2*$^{-/-}$ deficient fish brains compared to WT. GlcCer tended to be increased in livers and brains of *gba2*$^{-/-}$ zebrafish, while no significant reduction of GlcChol was measured in either *gba2*$^{-/-}$ or *gba1*$^{-/-}$*gba2*$^{-/-}$ samples (**Figure 2A** and **B**). The latter was unexpected, as zebrafish larvae (5 dpf) presented increased GlcCer levels and a reduction of GlcChol [27]. Moreover, GBA2 deficient mice accumulate GlcCer in their livers and show a decrease in GlcChol levels[20,21,23,25]. The chromatographic separation of GlcChol and GalChol revealed that the latter is significantly decreased in brains of *gba2*$^{-/-}$ and *gba1*$^{-/-}$*gba2*$^{-/-}$ fish compared to WT but not in *gba1*$^{-/-}$ or *gba1*$^{-/-}$*:asah1b*$^{-/-}$ brains.

Fatty acid composition of GSLs and SM

Neutral (glyco)sphingolipids consist of a sphingosine backbone linked to a fatty acid, which can differ in carbon chain length and presence of double bonds. Our routine LC-MS/MS method for sphingolipids contains a microwave-assisted deacylation step[29,30] and consequently renders no information on fatty acyl composition of measured sphingolipids. Another type of modified ceramide is sphingomyelin (SM), which has a phosphocholine headgroup and is the most predominant sphingolipid in cell membranes. However, phosphatidylcholine (PC) has similar m/z transitions as the SM species, including an identical daughter of 184.1 Da which is the phosphocholine headgroup of either SM or PC.

In order to study aberrant (glyco)sphingolipids with specific fatty acids, a LC-MS/MS procedure was developed using hydrophilic interaction liquid chromatography (HILIC) which enabled separation of sphingolipids with glucosyl- and galactosyl moieties as well as separation of SM and PC species. The ceramide species and the internal standard dihydroceramide eluted in the first 2 min, followed by GlcCer and GalCer lipids (2.5 to 3 min), LacCer (± 5 min), PC (± 8 min) and finally the more polar SM (± 9 min) (**Figure 3A**). First, the fatty acyl composition of ceramide, GlcCer, GalCer and SM species in WT brain was determined (**Figure 3B**). Ceramide species mainly had fatty acyls 16:0 (9.4%); 18:0 (24.6%); 24:0 (25.1%) and 24:1 (30.7%). In the brain, the main monohexosylceramide is GalCer (± 97%) (**Figure 2B**). The major fatty acyl species of GlcCer were 16:0 (61.2%) and 18:0 (13.8%), while GalCer mainly had the longer fatty acyls 22:0 (17.9%), 24:2 (10.1%), 24:1 (39.4%) and 24:0 (15.8%). SM mainly showed 16:0 (702.6 m/z, 30.7%), 18:0 (730.6 m/z, 16.5%) and 24:1 (812.7 m/z, 32.4%) fatty acyls.

However, in theory the composition of the double bonds on the sphingosine backbone and fatty acid of SM could be different due to the used phosphocholine headgroup as daughter in the LC-MS/MS method instead of the sphingosine backbone (264.4 m/z) for the other (glyco)sphingolipids. The fatty acyl composition of ceramide, GlcCer, GalCer and SM species in the liver was different from that of the brain (**Figure 3C**).

The majority of ceramide species in the liver had 16:0 (46.8 %) and 24:1 (21.8 %) fatty acyls, GlcCer predominantly contained 18:0 (81.1 %), while GalCer had comparable levels of 16:0 (23.7 %), 22:0 (27.3 %), 24:1 (23.7 %) and 24:0 (18.6 %) fatty acyls and SM predominantly 16:0 (48.9 %) fatty acyls with smaller fractions of 22:0, 22:1 and 24:1 (11.8%, 10.7% and 17.1 % respectively).

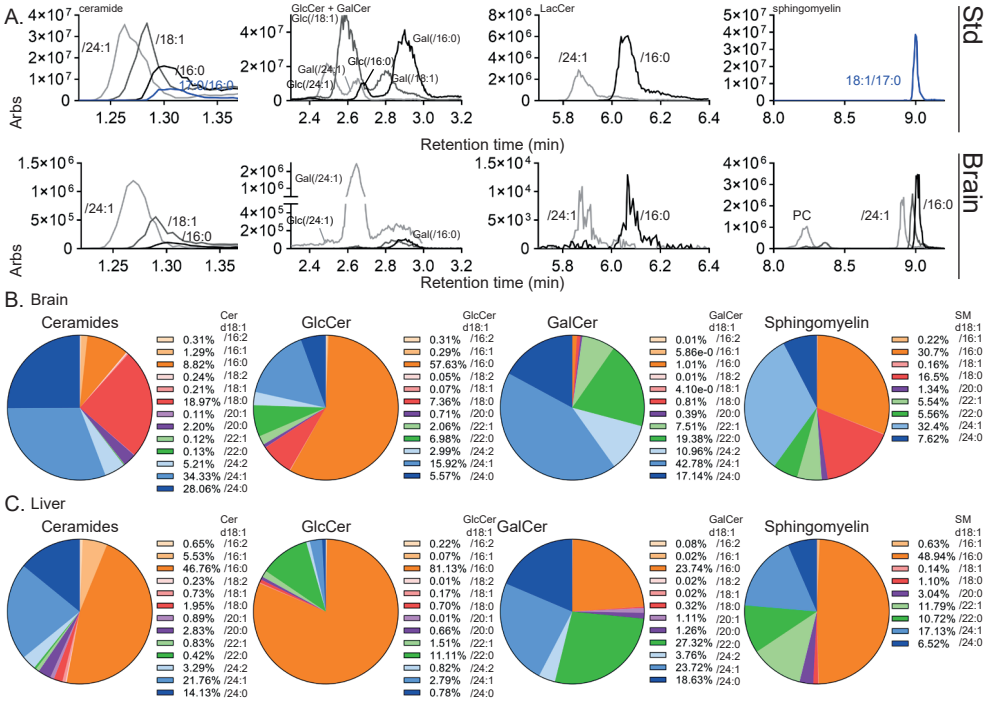

Figure 3 | LC-MS/MS method for analysis of neutral (glyco)sphingolipids with fatty acyl
(A) Combined chromatograms showing elution of different ceramides, GlcCer, GalCer, LacCer and sphingomyelin species from a sample with different standards (top panel) or a WT brain (bottom panel). The internal standards (dhCer d17:0/16:0 and SM d18:1/17:0) are shown in blue, lipids with 16:0 fatty acyl in black, 18:0 or 18:1 in grey and 24:1 fatty acyl in light grey. (Glyco)sphingolipids with different fatty acyl compositions were measured of WT brains **(B**) and livers **(C)** and depicted as ratio of the total of respective lipid species. WT, 12 wpf: n = 4

The same method was used to determine specific fatty acyl composition of sphingolipids in brain and liver of knockout zebrafish. A trend with regard to ceramide species was observed in brains of the *gba1*- and *gba1:asah1b* KO fish. Ceramide species with 16:0 and 18:0 fatty acyls appeared increased in *gba1*$^{-/-}$ and *gba1*$^{-/-}$*:asah1b*$^{-/-}$ brains, but only a significant increase of 16:0 was apparent in in *gba1*$^{-/-}$*:asah1b*$^{-/-}$ brain (± 6-fold, **Figure 4A**). In the liver, ceramide species with 16:0 and 18:0 ceramides were only significantly increased in *gba1:asah1b* KO fish (**Figure 4B**). Ceramides levels with longer fatty acyls (24:1, 24:0, 26:1 and 26:0) showed a slight, but not significant reduction in brains of *gba1*$^{-/-}$, *gba1*$^{-/-}$*:gba2*$^{-/-}$ and *gba1*$^{-/-}$*:asah1b*$^{-/-}$ zebrafish. SM showed a similar trend of increased 16:0 fatty acyls and decreased levels of longer fatty acyls, but none of the differences were significant (**Supplementary Figure 1A**).

All GlcCer species were increased in brain and liver of the three *gba1* mutant zebrafish. GlcCer with 18:0 and 20:0 fatty acyls showed the highest increase, while GlcCer species with 22:0 and 24:0 fatty acyls showed only small increases. Total GlcCer levels were not increased in *gba2*$^{-/-}$ brain and liver, however the GlcCer species with 18:0 and 20:0 fatty acids were significantly increased in brain of *gba2*$^{-/-}$ zebrafish. Brains of *gba1*$^{-/-}$*:gba2*$^{-/-}$ double mutant fish showed significant higher levels of GlcCer with 18:0 and 20:0 fatty acyls compared to single *gba1*$^{-/-}$ and *gba1*$^{-/-}$*:asah1b*$^{-/-}$ fish. LacCer, a product of GlcCer, also showed higher levels of species with 16:0 and 18:0 fatty acyls in the three *gba1* mutant zebrafish brains, consistent with increases of specific GlcCer species (**Supplementary Figure 1B**).

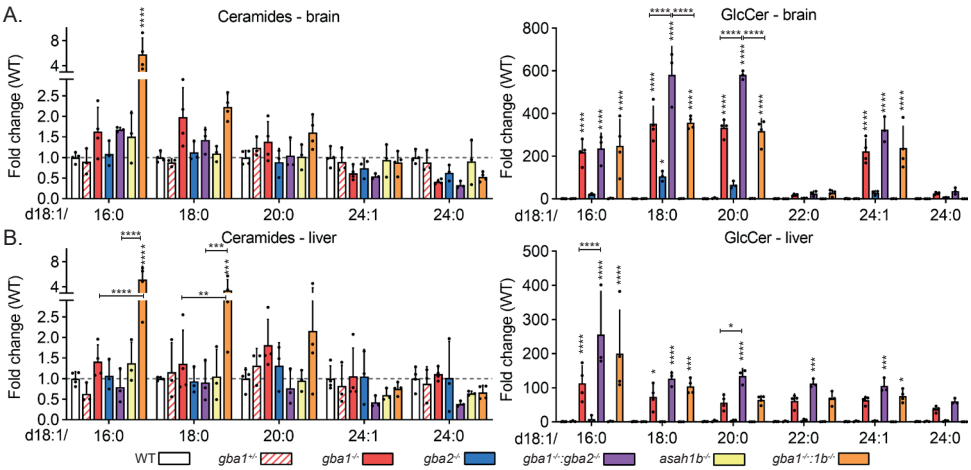

Figure 4| Changes in levels of ceramide and GlcCer with specific fatty acyls

Levels of ceramide and GlcCer species with different fatty acyls in brains **(A)** and livers **(B)** of WT (n = 4), *gba1*$^{+/-}$ (n= 3), *gba1*$^{-/-}$ (n = 4), *gba2*$^{-/-}$ (n = 3), *gba1*$^{-/-}$*:gba2*$^{-/-}$ (n = 3), *asa1b*$^{-/-}$ (n = 3) and *gba1*$^{-/-}$*:asah1b*$^{-/-}$ (n = 4). Ceramide and GlcCer species were measured and calculated as relative abundance in the target sample compared to the mean of the WT sample. Data is depicted as mean ± SEM. Data is analysed by Two-Way Anova with Tukey's multiple comparison test. In general, statistical comparisons are depicted of WT vs respective mutant, *gba1*$^{-/-}$ vs *gba1*$^{-/-}$*:gba2*$^{-/-}$, *gba1*$^{-/-}$ vs *gba1*$^{-/-}$*:asah1b*$^{-/-}$ or *gba1*$^{-/-}$*:gba2*$^{-/-}$ vs *gba1*$^{-/-}$*:asah1b*$^{-/-}$, only when a significant difference is apparent and relevant. Ns = not significant, * P < 0.05, ** P < 0.01, *** P < 0.001 and **** P < 0.0001.

Infiltration of Gaucher-like cells in visceral tissues during GCase deficiency

Zebrafish were sectioned along the sagittal plane and stained using haematoxylin and eosin (H&E) (**Figure 5** and **Supplementary Figure 2**). Infiltration of Gaucher-like cells was observed in liver (**5A**), spleen (**5B**) and pancreas (**5C**) of *gba1*$^{-/-}$ zebrafish (panels left down). The same was observed for tissues of *gba1*$^{-/-}$*:gba2*$^{-/-}$ and *gba1*$^{-/-}$*:asah1b*$^{-/-}$ fish, while no storage cells were observed in the tissues of *gba2*$^{-/-}$ zebrafish. No apparent abnormalities were observed in other tissues such as kidney, testis and skin (**Supplementary Figure 2**). One zebrafish with a gba1$^{-/-}$*:gba2*$^{-/-}$ background showed exceptionally very persistent infiltration of storage cells in liver, spleen, pancreas, kidney and testis (**Supplementary Figure 3**).

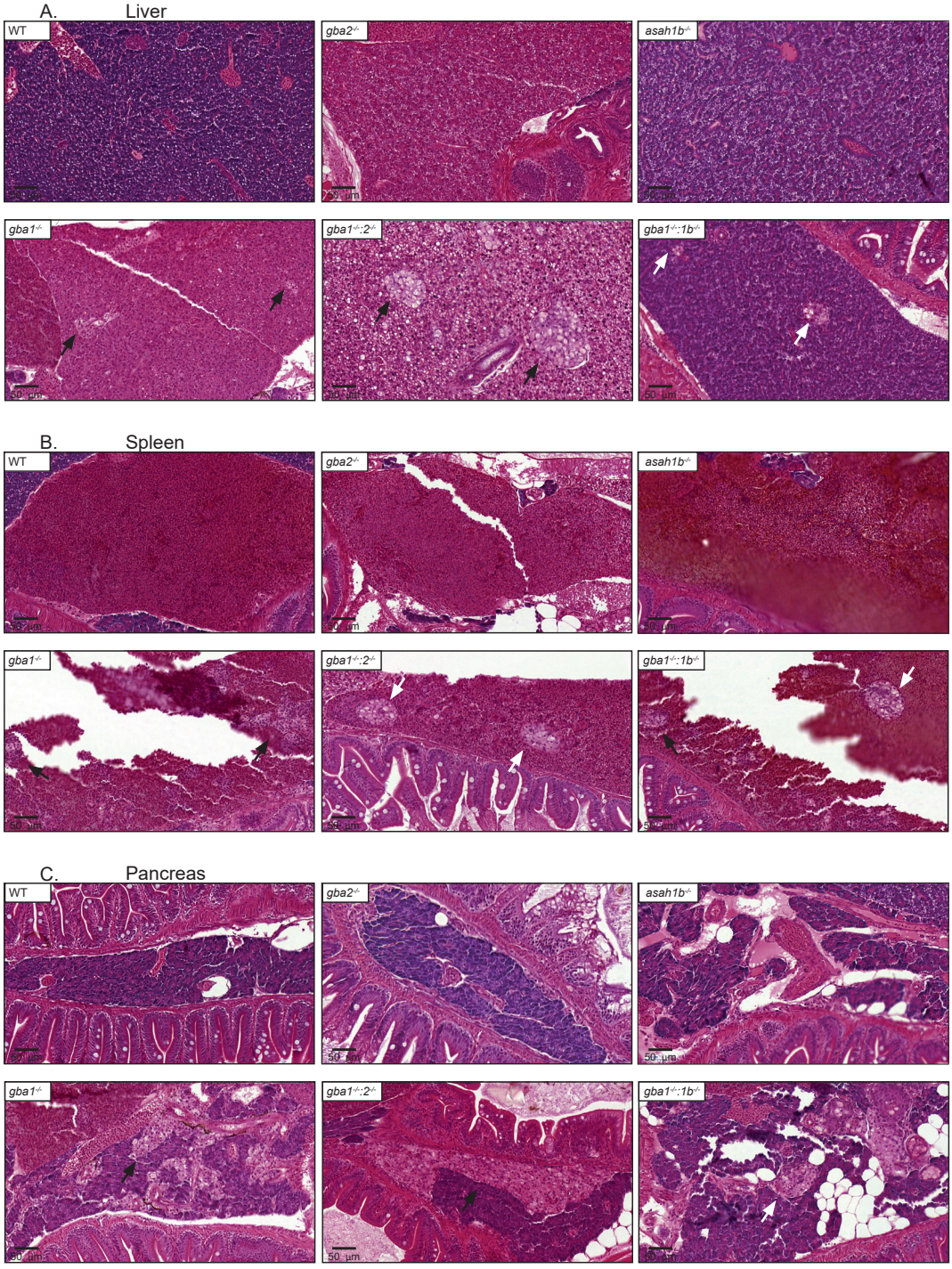

Figure 5 | Histopathology of visceral tissues

Haematoxylin and eosin (H&E) staining of liver **(A)**, spleen **(B)** and pancreas **(C)** of WT and mutant zebrafish. Gaucher-like cells are indicated with arrows.

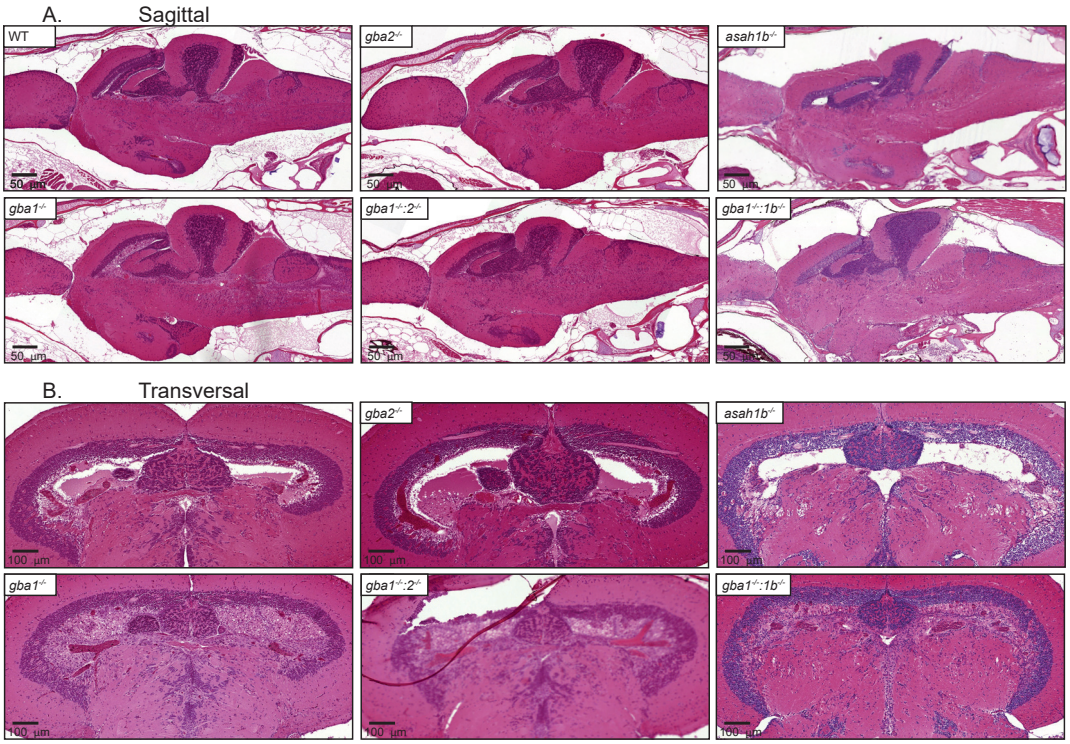

Figure 6| Histopathology of brain.
H&E staining of brain sagittal **(A)** and transversal sections **(B)** of WT and mutant zebrafish

Infiltration of Gaucher-like cells in brain during GCase deficiency

Next, brains were analysed for the presence of storage cells. No overt pathology was apparent in *gba1*$^{+/-}$ (carrier) brains and *gba2*$^{-/-}$ brains, while marked infiltration of Gaucher-like cells was observed in *gba1*$^{-/-}$*:gba2*$^{-/-}$ and *gba1*$^{-/-}$ and *gba1*$^{-/-}$ *:asah1b* brains (**Figure 6**). This infiltration was remarkably high in the periventricular grey zone of the optic tectum.

Neuroinflammation and neurodegeneration in *gba1:gba2* KO zebrafish

Brains were analysed for abnormal autophagy, storage cell presence, induction of lysosomes, inflammation, complement activation and neurodegeneration by analysis of the expression of relevant proteins and mRNAs. Upregulation of autophagy was evaluated by immunoblotting of p62, a ubiquitin-binding protein targeting other proteins for selective autophagy, and the two forms of LC-3, cytosolic LC3-I and lipid conjugate LC3-II which is recruited to autophagosomal membranes. *Gba1*$^{-/-}$, *gba1*$^{-/-}$*:gba2*$^{-/-}$ and *gba1*$^{-/-}$*:asah1b*$^{-/-}$brains showed increased levels of LC3-II and p62, indicating increased autophagy (**Figure 7A** and **B**). Consistent with upregulation of the lysosomal-autophagy pathway, increased expression of the lysosomal protease *catd* was observed in all of the gba1$^{-/-}$ brains. In analogy to the histopathology examination (**Figure 6**), mRNA levels of storage cell biomarkers *gpnmb* and *chia.6* were increased in all of the gba1$^{-/-}$ brains (**Figure 7C**).

The same was observed for genes involved in neuroinflammation, such as *il-1ß, tnfß*, the gene for the microglia marker *apoeb* and genes involved in the complement system *c1qA*, *c3.1* and *c5aR (***Figure 7C**). Of note, no significant difference was found between *gba1*$^{-/-}$ and *gba1*$^{-/-}$*:gba2*$^{-/-}$ for any of the studied proteins or genes.

The study described in chapter 6 suggested a potential harmful role for GlcSph in accelerating dopaminergic neuronal loss. Indeed, *gba1*$^{-/-}$*:asah1b*$^{-/-}$ fish lacking excessive GlcSph as compared to *gba1*$^{-/-}$ fish show a significantly improved expression of mRNAs encoding the tyrosine hydroxylase (*th1*), indicative for dopaminergic neurons, as well as improved expression the two zebrafish synuclein orthologues, *sncß* and *sncγb* (**Figure 7C**). Brains of *gba1*$^{-/-}$*:gba2*$^{-/-}$ zebrafish with excessive GlcSph showed a significant reduction of *th1, sncß* and *sncγb* mRNAs like *gba1*$^{-/-}$ fish (**Figure 7C**). In all three *gba1* mutant brain a reduction of the transcript encoding myelin-binding protein *(mbpa*) was observed. Thus, no protective effect by the combined GBa2 deficiency in this respect was observed.

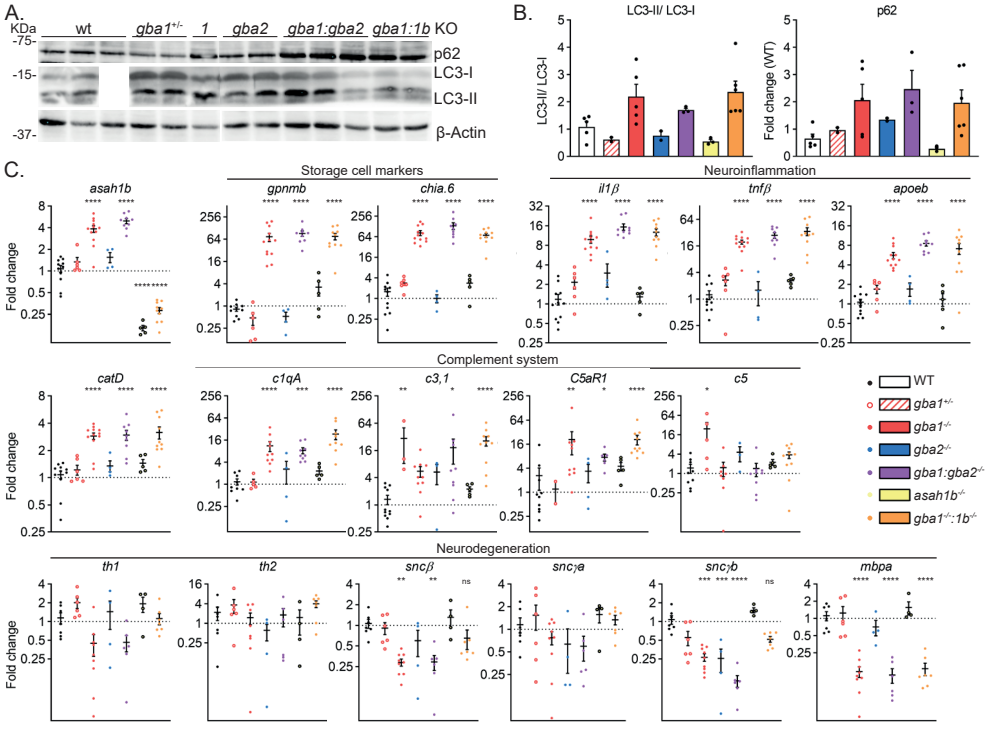

Figure 7| Protein and RNA abnormalities in WT and knockout zebrafish

(A) Representative western blots of p62, LC-3 and β-actin as loading control. **(B)** Quantification of protein abnormalities with the ratio of LC-3II/LC-3I and ratio of p62/WT (n = 2-5). **(C)** mRNA levels of *asah1a, asah1b, gpnmb*, *chia.6*, *il-1ß*, *tnfß*, *apoEb, catD, c1qA, c3.1, c5aR*, *c5, th1, th2, sncß, snγa, sncγb* and *mbpa* were determined using RT-qPCR analysis of n = 5- 11 fish. Data is normalized using two housekeeping genes (*ef1α* and *rpl13*), analysed by One-Way Anova with Tukey's multiple comparison test or Brown-Forsythe and Welch Anova with Dunnett's multiple comparisons test for *gpnmb* and *chia.6*and depicted as scattered dot plot ± SEM. * P < 0.05, ** P < 0.01, *** P < 0.001 and **** P < 0.0001.

Unpredictable disease progression of *gba1:gba2* deficient zebrafish

The *gba1*$^{-/-}$ zebrafish develop a progressive phenotype and it was necessary to cull individual fish before the experimental end point of 12 wpf (see chapter 6). In contrast, *gba1*$^{-/-}$:a*sah1b*$^{-/-}$ *fish* lacking excessive GlcSph developed similar phenotypic symptoms at later age, around 15-17 wpf (**Figure 8A**). Most *gba1*$^{-/-}$ zebrafish developed a characteristic drop of the tail prior to the change in swimming behaviour. In this respect, *gba1*$^{-/-}$*:gba2*$^{-/-}$ zebrafish showed a very unpredictable course of disease manifestations. The change in swimming behaviour could occur in only a matter of days and was not preceded by a drop in the tail. Many *gba1*$^{-/-}$*:gba2*$^{-/-}$ fish had to be sacrificed earlier than their *gba1*$^{-/-}$ counterparts, at approximately 10-11 weeks (**Figure 8A**). No abnormal morphology was observed for the *gba1*$^{+/-}$ (carrier), *gba2*$^{-/-}$, *asah1b*$^{-/-}$ and *gba1*$^{-/-}$*:asah1b*$^{-/-}$ fish at 12 wpf (**Figure 8B** and **C**). Both *gba1*$^{-/-}$ and g*ba1*$^{-/-}$*:gba2*$^{-/-}$ fish were significantly smaller and more curved than WT or gba1$^{-/-}$:asah1b$^{-/-}$ fish (**Figure 8B** and **C**), while *gba1*$^{-/-}$ and *gba1*$^{-/-}$*:gba2*$^{-/-}$ age-matched fish appeared comparable (t= 10, 11 and 12 wpf; **Supplementary Figure 4**).

Swimming patterns

All zebrafish were individually filmed at 12 wpf, or at the end stage of their lives, to quantify their swimming pattern (**Figure 8D** and **E**). Most *gba1*$^{-/-}$ zebrafish and *gba1*$^{-/-}$*:gba2*$^{-/-}$ zebrafish failed to maintain un upright position, while some severe *gba1*$^{-/-}$*:gba2*$^{-/-}$ individuals were swimming upside down complicating their tracking (**Figure 8D**). A significant reduction in velocity was observed for *gba1*$^{-/-}$*:gba2*$^{-/-}$ zebrafish compared to WT and *gba1*$^{-/-}$ zebrafish (**Figure 8D** and **E**). Noteworthy, the tracked Gba1:Gba2 double mutant zebrafish showed movement throughout the tank, in contrast to the significant increase of time spend at the bottom of the tank by *gba1*$^{-/-}$ zebrafish (**Figure 8D** and **E**).

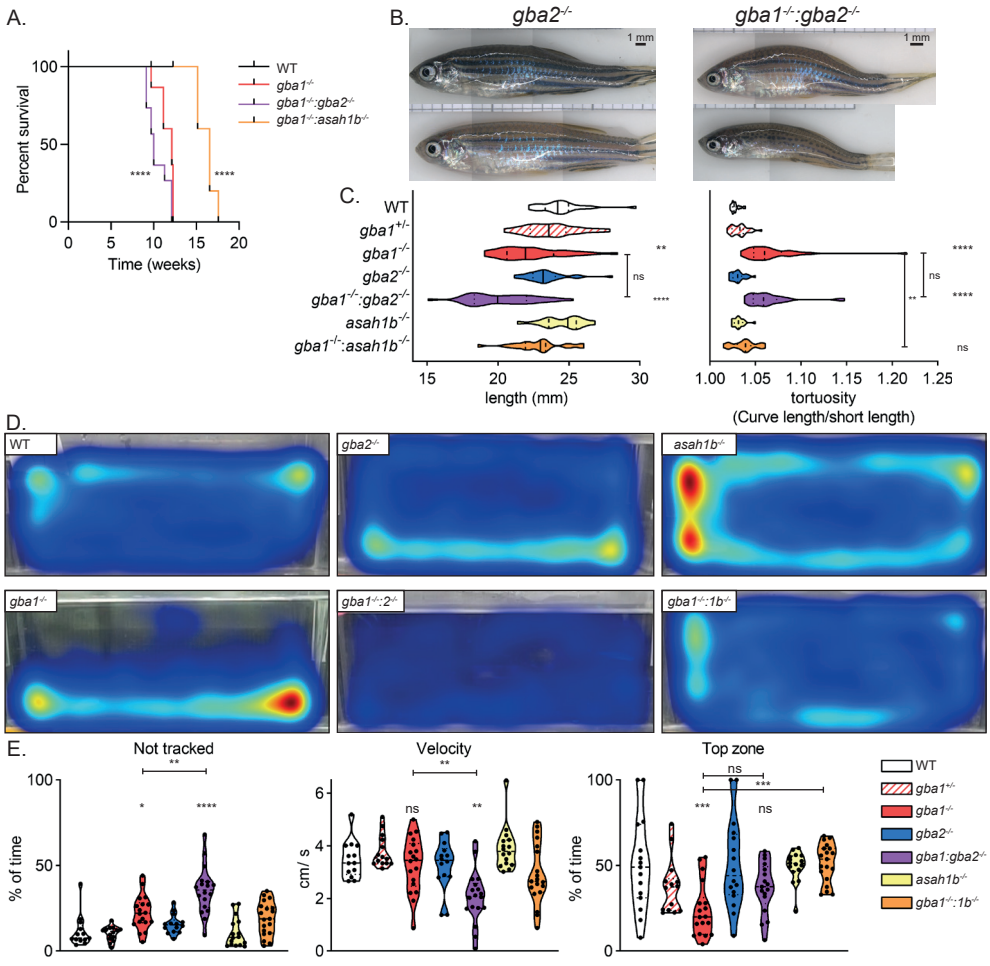

Figure 8| Morphology phenotype and change in behaviour of *gba1*$^{-/-}$ and *gba1*$^{-/-}$:gba2$^{-/-}$ zebrafish

(A) Kaplan-Meier plot for the onset of predetermined symptoms; *gba1*$^{-/-}$ (n = 29), *gba1*$^{-/-}$:*gba2*$^{-/-}$ (n = 30) and *gba1*$^{-/-}$:*asah1b*$^{-/-}$ (n = 5). Curves of *gba1*$^{-/-}$:*gba2*$^{-/-}$ and *gba1*$^{-/-}$:*asah1b*$^{-/-}$ were compared to the curve of *gba1*$^{-/-}$ and analysed using a Log-rank (Mantel-Cos) test. **(B)** Representative photographs of *gba2*$^{-/-}$ and *gba1*$^{-/-}$:*gba2*$^{-/-}$ zebrafish. **(C)** The length of individual zebrafish, head to tail base, is determined as well as the tortuosity, calculated as ratio of the length along the back divided by the length of the fish. Data of individual zebrafish is depicted in a violin plot; WT (n= 21), *gba1*$^{+/-}$ (n = 28), *gba1*$^{-/-}$ (n = 29), *gba2*$^{-/-}$ (n = 23), *gba1*$^{-/-}$:*gba2*$^{-/-}$ (n = 30), *asah1b*$^{-/-}$ (n = 16), *gba1*$^{-/-}$:*asah1b*$^{-/-}$ (n = 19) and analysed using a non-parametric Kruskal-Wallis test with Dunn's multiple comparison's test. **(D)** Representative movement traces recorded at 12 wpf, except for the 10 wpf *gba1*$^{-/-}$:*gba2*$^{-/-}$. Red indicates more time and blue less time spend at that location. **(E)** Quantification of the movement traces of individual zebrafish, including the time (%) unable to track individual zebrafish, the average velocity (in cm/s) and time spend in the top half of the tank (%). Data of individual zebrafish is depicted in a violin plot; WT (n= 13), *gba1*$^{+/-}$ (n = 14), *gba1*$^{-/-}$ (n = 16), *gba2*$^{-/-}$ (n = 14), *gba1*$^{-/-}$:*gba2*$^{-/-}$ (n = 18), *asah1b*$^{-/-}$ (n = 16), *gba1*$^{-/-}$:*asah1b*$^{-/-}$ (n = 19) and analysed using One-Way Anova with Tukey's multiple comparison's test. In general, statistical comparisons are depicted of WT vs respective mutant, *gba1*$^{-/-}$ vs *gba1*$^{-/-}$:*gba2*$^{-/-}$ or *gba1*$^{-/-}$ vs *gba1*$^{-/-}$:*asah1b*$^{-/-}$ only when a significant difference is apparent and relevant. Ns = not significant, * P < 0.05, ** P < 0.01, *** P < 0.001 and **** P < 0.0001.

GCase deficient juveniles accumulate GSLs, but show no obvious phenotype

Overall, a more severe and unpredictable phenotype was observed for the *gba1*$^{-/-}$*:gba2*$^{-/-}$ zebrafish compared to the *gba1*$^{-/-}$ zebrafish, even though at the end stage no significant biochemical differences were observed in lipid abnormalities or physiological processes such as autophagy and neuroinflammation. Therefore, fish were also examined at earlier developmental stages, when the phenotype was not apparent yet. Up to 8 wpf no significant difference in size (**Figure 9A,** 4 and 8 wpf) or curvature of the back (tortuosity in **Figure 9B,** 4 and 8 wpf) was apparent and no abnormal swimming behaviours were observed in any of the groups. Only at the end of the experiment (12 wpf maximal), *gba1*$^{-/-}$ and *gba1*$^{-/-}$*:gba2*$^{-/-}$ zebrafish were significantly smaller and more curved than WT (**Figure 9**, end stage).

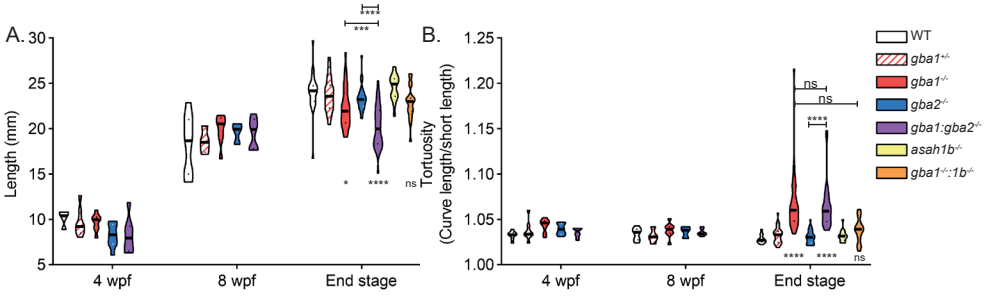

Figure 9 | Morphology of juvenile zebrafish at different ages

(A) Length **(B)** Tortuosity WT (white bars: 4 wpf, n = 9; 8 wpf, n= 8; end stage, n= 23), *Gba1*$^{+/-}$ (red, striped bars: 4 wpf, n = 9; 8 wpf, n = 4; end stage, n= 28), *gba1*$^{-/-}$ (red bars: 4 wpf, n= 8; 8 wpf, n = 8; end stage, n = 29), *gba2*$^{-/-}$ (blue bars: 4 wpf, n = 9; 8 wpf, n = 3; end stage, n = 26), *gba1*$^{-/-}$*:gba2*$^{-/-}$ (purple bars: 4 wpf, n = 8; 8 wpf, n = 7; end stage n = 30). Data is depicted as violin plot, with the mean as black line and quartiles as dashed lines and analysed using a two-way ANOVA with Tukey's multiple comparison test. Ns = not significant, * < 0.05, *** P < 0.001 and **** P < 0.0001.

Abnormalities in head and body region in developing fish.

Head and body regions of zebrafish of different age were separated to analyse glycosphingolipid, protein and RNA changes. At 2 and 4 wpf the juvenile fish were too small to dissect distinct organs, while, at 8 and 12 wpf, homogenates of distinct organs could be prepared. Lipid analysis revealed that GlcSph had accumulated in head and body samples of *gba1*$^{-/-}$ and *gba1*$^{-/-}$*:gba2*$^{-/-}$ fish of all developmental ages, as observed for 5 dpf larvae and adult organs (**Figure 10A**). As in the 5 dpf zebrafish larvae, GlcSph levels in the *gba1:gba2* KO fish appeared somewhat higher than in *gba1* KO counterparts but no significant and progressive trend was observed. Total GlcCer was slightly, but not significantly, increased in *gba1*$^{-/-}$ zebrafish of 2 wpf and significantly increased in 2 wpf *gba2*$^{-/-}$ and the *gba1:gba2* double mutant zebrafish (**Figure 10B**). The lack of significant GlcCer accumulation was also described for the 5 dpf *gba1*$^{-/-}$ larvae, which was attributed to the deposition of maternal RNA and protein in the yolk (Chapter 6). However, at the age of 2 wpf it is not likely that maternally derived GCase is still highly present.

GlcCer levels of *gba1*$^{-/-}$ and *gba1*$^{-/-}$*:gba2*$^{-/-}$ zebrafish showed a progressive increase at 4 wpf and 8 wpf, while GlcCer levels of *gba2*$^{-/-}$ zebrafish did not increase further. GlcCer accumulation was more profound in the head region of 4 wpf and 8 wpf *gba1*$^{-/-}$ and *gba1*$^{-/-}$*:gba2*$^{-/-}$ zebrafish compared to the body region.

GlcChol levels of *gba1*$^{-/-}$ zebrafish became significantly increased in the brain at 8 wpf and 12 wpf (**Figure 9C**), indicating that GCase is important for the lysosomal hydrolysis of GlcChol. A reduction in GlcChol levels was reported in the 5 dpf larvae with a Gba2 deficient background, consistent with the ability of Gba2 to synthesize GlcChol as transglucosidase[27]. Surprisingly, none of the older *gba2*$^{-/-}$ or *gba1*$^{-/-}$:*gba2*$^{-/-}$ zebrafish showed a prominent difference in GlcChol levels compared to WT (**Figure 10C**). A possible explanation for this discrepancy might involve the presence of glucosylated sterols in the provided plant-based food starting from the 5 dpf timepoint reported before. The detected GlcChol in the zebrafish might, therefore, stem largely from the exogenous source.

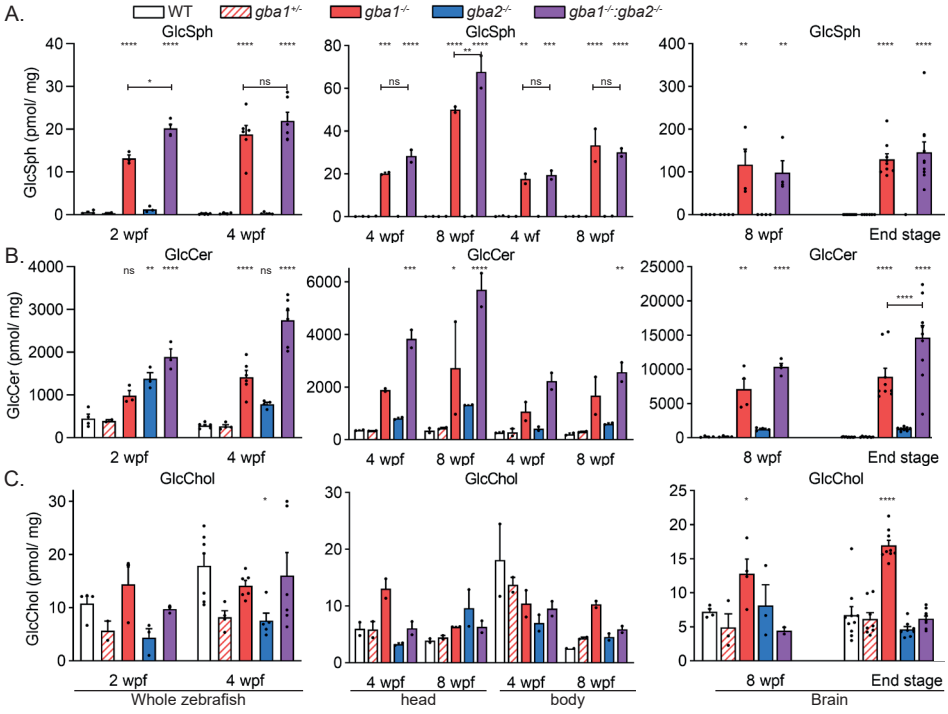

Figure 10 | Relevant glycosphingolipids of juvenile zebrafish at different ages
GlcSph (A), GlcCer (B) and GlcChol (C) were measured of whole zebrafish at 2 and 4 wpf (left), head and body regions at 4 and 8 wpf (middle) and brains of 8 wpf and end stage fish (right). Whole fish: 2 wpf (n = 2-4); 4 wpf (n = 4-7), Head/body: 4 wpf (n= 2); 8 wpf (n = 2) and brains: 8 wpf (n = 3-4); end stage (n = 8-12). Data is depicted as mean ± SEM and analysed using a two-way ANOVA with Tukey's multiple comparison test.

Development of neuropathology.

Glycosphingolipid abnormalities are already detectable in GCase-deficient zebrafish at a few dpf and increase progressively, while phenotypic manifestations become detectable only at much older age. The progression of neuroinflammation was therefore analysed in developing zebrafish by measurement of protein and RNA abnormalities in head (4 and 8 wpf) and brain (8wpf) region. The p62 marker of autophagy was found to be low in WT, *gba1*$^{+/-}$ and gba2$^{-/-}$ samples at 4 and 8 wpf, but increased in samples of all fish with a GCase deficiency (**Figure 11A** and **B**). The storage-cell biomarker *chia.6* was already significantly increased at 8 wpf in brains of GCase-deficient fish, with *gpnmb* levels showing a similar

trend (**Figure 11C**). Transcript levels of the lysosomal protease *catD* and microglia marker *apoeb* were also significantly increased in 8 wpf brain, as well as the inflammation markers *il1β* and *tnfβ* (data not shown). Expression of complement components *c1qA* and *c3.1* was slightly, but not significantly increased at 8 wpf. At the same age, a reduction of mRNA levels of *th1, sncβ* and *snγb* was apparent, however only the reduction of *sncβ* and *snγb* levels in *gba1*$^{-/-}$*:gba2*$^{-/-}$ brains reached significance. Overall, the protein and mRNA analyses indicate that neuroinflammation and autophagy already becomes abnormal at 8 wpf, clearly before the onset of morphological and behaviour disease manifestation, while genes related to neurodegeneration were not significantly reduced yet at this age.

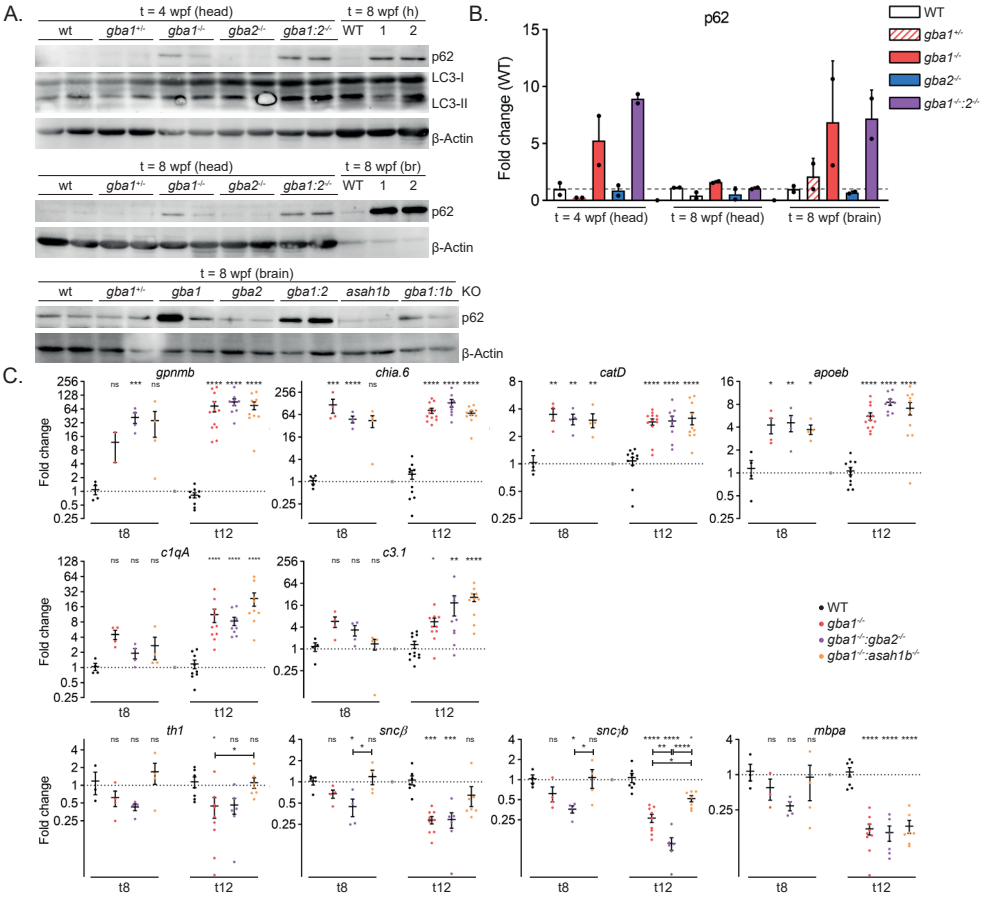

Figure 11 | Protein and RNA abnormalities in WT and knockout zebrafish

(A) Representative western blots of p62, LC-3 and β-actin as loading control of head regions (h) at 4 wpf and 8 wpf or dissected brains (br) at 8 wpf. **(B)** Quantification of protein abnormalities with the ratio of p62/WT (n = 2-4). **(C)** mRNA levels of *asah1a, asah1b, gpnmb, chia.6, il-1β, tnfβ, apoEb, catD, c1qA, c3.1, c5aR, c5, th1, th2, sncβ, snγa, sncγb* and *mbpa* in brains of 8 wpf or 11 wpf zebrafish were determined using RT-qPCR analysis of n = 2 for *gpnmb, gba1*$^{-/-}$ and n = 4- 11 fish for others. Data is normalized using two housekeeping genes (*ef1α* and *rpl13α*), analysed by One-Way Anova with Tukey's multiple comparison test or Brown-Forsythe and Welch Anova with Dunnett's multiple comparisons test for *gpnmb* and *chia.6*and depicted as scattered dot plot ± SEM. In general, statistical comparisons are depicted of WT vs respective mutant, *gba1*$^{-/-}$ vs *gba1*$^{-/-}$*:gba2*$^{-/-}$, *gba1*$^{-/-}$ vs *gba1*$^{-/-}$*:asah1b*$^{-/-}$or *gba1*$^{-/-}$*:gba2*$^{-/-}$ vs *gba1*$^{-/-}$*:asah1b*$^{-/-}$, only when a significant difference is apparent and relevant. Ns = not significant, * P < 0.05, ** P < 0.01, *** P < 0.001 and **** P < 0.0001.

Discussion

The ubiquitous glycosphingolipid GlcCer is degraded by cells in their lysosomes by the acid β-glucosidase GCase or in the cytosolic membrane leaflet by the membrane-associated GBA2. Deficiency of GCase in humans leads to the lysosomal storage disorder GD. Little is presently known about the impact of GBA2 during impaired lysosomal degradation of GlcCer. GCase deficiency in humans is not only accompanied by accumulation of GlcCer, but also the formation of excessive GlcSph by lysosomal acid ceramidase (ACase). In addition, accumulation of glucosylated cholesterol (GlcChol) during GCase deficiency is reported[25]. GlcChol is typically synthesized by GBA2 via a transglucosylation reaction using GlcCer as sugar donor and normally degraded by GCase to cholesterol and glucose[25]. The potential contribution of the excessive GlcCer, GlcSph and GlcChol during GCase deficiency to specific symptoms is poorly understood at present. To generate new insights, mutant zebrafish were generated by CRISPR/Cas9 with a knockout (KO) of the *gba1, gba2* and *asah1b* genes encoding respectively GCase, GBA2 and the ACase responsible for formation of GlcSph. The present study primarily focussed on a comparison of *gba1*$^{-/-}$, *gba1*$^{-/-}$*:gba2*$^{-/-}$ and *gba1*$^{-/-}$*:asah1b*$^{-/-}$ fish up to the adult age of 12 weeks. In addition, adult carrier *gba*$^{+/-}$, *gba2*$^{-/-}$ and *asah1b*$^{-/-}$ zebrafish were studied. An overview of findings of the different zebrafish is given in **Supplementary Table 1**.

First of all, attention was paid to lipid abnormalities in the various mutant zebrafish. GlcCer accumulated in *gba1*$^{-/-}$ fish relatively late. The fish showed at young age (up to 2 wpf) little accumulation of GlcCer. The lipid levels of GlcCer became significantly increased at 4 wpf. The *gba1*$^{+/-}$ carrier fish showed no GlcCer abnormalities whatsoever up to 12 wpf. The *gba2* KO fish developed an increase of GlcCer in the brain, specifically the species with a 18:0 fatty acyl, but total GlcCer increase was statistically not significant. An increase of HexCer 18:0 was also reported for cerebellum of GBA2-deficient mice, where again the increase of total HexCer did not reach significance[21]. Interestingly, total GlcCer levels were only significantly increased in young Gba2 deficient zebrafish (0-2 wpf) and decreased thereafter, in contrast to the GCase-deficient fish. This finding might indicate that the GlcCer catabolism by Gba2 is relatively higher in young zebrafish. The mutant *gba1:gba2* fish was striking with respect to the increase in GlcCer. In brain there was a prominent increase of GlcCer with 18:0 and 20:0 fatty acyls was observed, exceeding that observed in *gba1*$^{-/-}$ brains. Increased levels of these specific GlcCer species were also observed in brains of *gba2* KO fish, therefore it is likely that these species of GlcCer accumulate in the cytosol due to the concurrent Gba2 deficiency. In the liver, GlcCer 16:0 was markedly increased, again exceeding the abnormality in the same lipid in *gba1*$^{-/-}$ fish. The total GlcCer increase in *gba1:gba2* double KO fish already was significant at the age of 1 wpf[27] and GlcCer levels tended to be at all ages the highest among all genotypes. Finally, gba1$^{-/-}$:asha1b$^{-/-}$ fish were quite comparable to *gba1*$^{-/-}$ fish in their GlcCer abnormalities in brain and liver.

GlcSph started to accumulate in *gba1*$^{-/-}$ fish and *gba1*$^{-/-}$*:gba2*$^{-/-}$ fish at very young age (before 5 dpf as described in chapter 5[27]) and these levels increased over time. GlcSph levels tended to be higher in *gba1*$^{-/-}$*gba2*$^{-/-}$ fish than *gba1*$^{-/-}$ fish at various ages, however these differences never reached significance. Slightly elevated GlcSph levels were earlier also detected in spleens of mice with GCase deficiency in hematopoietic cells with or without a GBA2 deficiency[23]. The *gba1*$^{+/-}$ (carrier) fish and *gba2*$^{-/-}$ fish showed no accumulation of GlcSph, while brains and livers of *gba1*$^{-/-}$*:asah1b*$^{-/-}$ fish showed no GlcSph at 12 wpf because of their Asah1b deficiency as described in chapter 6.

GlcChol levels increased from 4 wpf in *gba1*$^{-/-}$ fish and were significantly increased in the brains of 8 and 12 wpf fish. An unexpected finding was the similar GlcChol level in Gba2 deficient fish compared to WT. In mice and larvae different observations in this respect have been made. Adult GBA2 deficient mouse livers and Gba2 deficient larvae (up to 5 dpf) were found to show a reduced GlcChol[25,27], consistent with the role of Gba2 in synthesis of GlcChol. Reduced GlcChol levels were detected in developing Gba2 deficient zebrafish until the age of 4 wpf, but levels became quite comparable to WT at 8 and 12 wpf. A possible explanation for these findings might be offered by the zebrafish diet and its lipid composition. Glucosylated sterols are present in various plants[31], although campesterol, sitosterol and stigmasterol are the main types of sterols found in plants[32]. Next to the manufactured, plant-based food, zebrafish also receive food of animal origin starting at the age of 5 dpf life. This to provide optimal and consistent rates of survival and growth during larval rearing and promote natural active feeding behaviour[33,34]. The larvae are fed with *Brachionus plicatilis* (rotifers), an aquatic invertebrate species, from 5 dpf to 2 weeks of age, while juveniles and adults receive A*rtemia*, a genus of small aquatic crustaceans. At present, no lipid measurements of these food sources have been performed, however it is conceivable that the animal food could contain glucosylated sterols which are taken up by the developing zebrafish.

The absence of a clear phenotype of the adult Gba2-deficient fish is remarkable in view of the findings made with rodents regarding male infertility associated with Gba2 deficiency [20-22] and the observed association of GBA2 defects with neurological complications in some individuals[21]. The Gba2-deficient fish did not show abnormal fertility: a regular sized tank of *gba2* KO adults produced average clutches with normally developing larvae, comparable to WT fish. Of note, in the present study lipid levels in the testis and sperm morphology were not analysed. The g*ba2* KO fish were maintained for many months without symptoms. The fish only showed aging features after 2 years, comparable to the WT strains. In sharp contrast, HSP and ARCA patients with mutations in *GBA2* develop a progressive neurological phenotype, including muscle weakness and spasticity, with an early onset in infancy or childhood[8,10]. GBA2-knockout mice develop mild defects in the gait pattern, but strong locomotor defects were only observed in a few individuals[21]. Overall, Gba2-deficient zebrafish appear to have similar biochemical results to the reported GBA2 knockout mice, including an increase in specifically GlcCer d18:1/18:0, while the lifespan and lack of a clear phenotype contrasts with patients carrying mutations in *GBA2* and with GBA2-deficient mice showing male infertility.

The impact of the enzyme Gba2 during deficiency of GCase in zebrafish warrants discussion. Two studies with mice with a reduced GCase activity (conditional GCase deficiency in hematopoietic cells and secondary GCase deficiency in NPC1 mutants) reported amelioration of some symptoms in animals by concomitant GBA2 deficiency[23,24]. Comparison of the findings made with *gba1*$^{-/-}$ and *gba1*$^{-/-}$*:gba2*$^{-/-}$ zebrafish is therefore of interest. The *gba1* KO zebrafish showed a clear onset and progression of symptoms, starting with a drop in the tail, followed by postural imbalance and a change in swimming behaviour. In contrast, g*ba1:gba2* double KO fish showed an unpredictable course of disease manifestation and no clear characteristic drop of the tail was observed as onset. Severe postural imbalance and abnormal swimming behaviour could be observed in only a matter of days, with some individual fish starting to swim upside down overnight. *Gba1:gba2* KO fish were culled earlier than single *gba1* KO fish and the decreased lifespan and quality of life of most *gba1:gba2* KO fish was unexpected. It should be taken in mind the studied fish are complete knockouts in both enzymes, contrary to the mouse models mentioned above. In the type 1 GD mice, GCase was functional in the neuronal lineage. In the NPC1 model, GCase deficiency is only partial and the animals have a far less severe disease progression than neuronopathic GD mice lacking GCase in neuronal cells (life spans of 85 vs 21 days for NPC1 knockout[24] and nestin:Cre:GD mice respectively[19]). Consistently, GlcCer and GlcSph levels in brain of 85 day old NPC1 mice are lower than in 21 day old neuronopathic GD mice (GlcCer: 311 pmol/mg wet weight vs 338 pmol/mg tissue and GlcSph: 1.4 pmol/mg wet weight vs 28 pmol/mg tissue[17,24]).

The mechanisms underlying the onset, progression and severity of symptoms in GCase-deficient zebrafish are puzzling. The present study indicates that the presence of storage cells, neuroinflammation, and impairment of autophagy is comparable in the brains of *gba1-*, *gba1:gba2-* and *gba1:asah1b* KO fish while the latter animals have a much milder phenotype. Storage cells, neuroinflammation and impaired autophagy were already apparent in brains of all GCase-deficient zebrafish at 8 wpf, clearly prior to the onset of phenotypic symptoms. Dopaminergic neuronal cell loss likely underlies some of the observed neurological complications in the mutant zebrafish. The expression of mRNAs coding for tyrosine hydroxylase (*th1*), a protein required for formation of dopamine, and two synuclein genes (*sncβ* and *sncγb*) was found to be significantly reduced in brains of *gba1 KO* and *gba1:gba2* KO fish at 10-12 wpf, but not in those of *gba1:asah1b* KO fish. These important findings need confirmation at protein level by immunohistochemistry. In addition, it will be important to study more closely (activated) microglia in the mutant zebrafish. A prominent role for microglia activation and astrogliosis in neuronal loss occurring in neuropathic Gaucher mice has been proposed by Futerman and co-workers[35,36]. This process would be driven by GlcCer accumulation according to these investigators[35,37]. It has recently been reported that Gpnmb is a marker for activated microglia in neuronopathic GD mice and is also elevated in cerebral spine fluid from type 3 GD patients[38]. *Gpnmb* mRNA levels are also increased in mutant zebrafish but this does not correlate with the course of neurodegeneration or phenotypic manifestations.

To conclude, at present it remains unclear whether exposure to excessive GlcSph in zebrafish drives dopaminergic neuronal loss after some time or whether microglia activation, driven by GlcCer accumulation, is a driving force for neurodegeneration. It is *a priori* conceivable that both processes occur hand in hand and that the sequence and importance of pathology events differs among species. In fact, it is known that the consequences of pharmacologically induced GCase deficiency in different mice strains with conduritol B-epoxide (CBE) may differ dramatically[39]. It was observed that the age of survival following CBE administration varied from 40 to 200 days. It can be argued that toxic activated microglia will likely promote loss of dopaminergic neurons and subsequent symptomatology and excessive GlcSph may speed up such events.
Likewise, spatio-temporal assessment of GlcSph and specifc GlcCer species in brain regions may be of value. Various mass spectrometry-based imaging techniques for this purpose are presently developed and applied. A recent study reported a correlation of GlcCer d18:1/18:0 accumulation with microglia activation in brain of neuronopathic GD mice[40]. Of particular interest will be correlation of lipids with complement-activating immune complexes deposited on neuronal cells, oxidative stress and mitochondrial dysfunction[37,41-43].

In conclusion, the comparative investigation of *gba1-*, *gba1:gba2-* and *gba1:asah1b* KO fish provided new insights as well as questions regarding pathology induced during GCase deficiency. It is apparent that excessive GlcSph is associated with more severe disease manifestation but the role of microglia activation and neuroinflammation warrants further investigation. The role of excessive GlcChol could not be elucidated since adult *gba1:gba2* KO fish did unexpectedly not show reduced levels of GlcChol in their brains.

Acknowledgements

Joost Willemse is kindly acknowledged for the ImageJ plugin to quantify the length and tortuosity of individual zebrafish. Sophie Gerhardt and Saskia Maas are acknowledged for the histology procedures and Daniela Salvatori for the pathological examination. Ernst Bijk, Claire de Wit and Christian Tudorache are kindly acknowledged for their work on tracking and quantifying zebrafish movements. The study was supported by the NWO BBOL 2018 (737.016.022) grant.

Supplementary Information

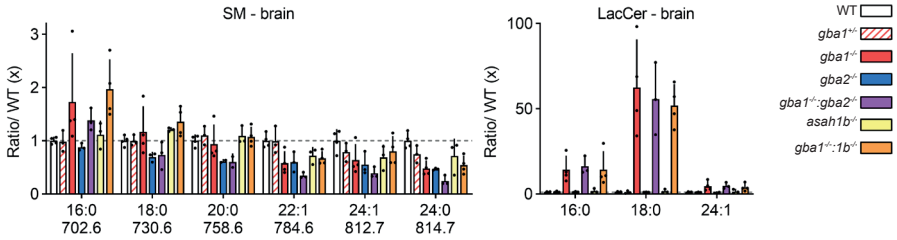

Supplementary Figure 1 | Levels of SM and LacCer with different fatty acids in brains of WT (n = 4), *gba1*$^{+/-}$ (n= 3), *gba1*$^{-/-}$ (n = 4), *gba2*$^{-/-}$ (n = 3), *gba1*$^{-/-}$:*gba2*$^{-/-}$ (n = 3), *asa1b*$^{-/-}$ (n = 3) and *gba1*$^{-/-}$:*asah1b*$^{-/-}$ (n = 4). Lipid species were measured, calculated and analysed as described in the experimental procedures. * P < 0.05

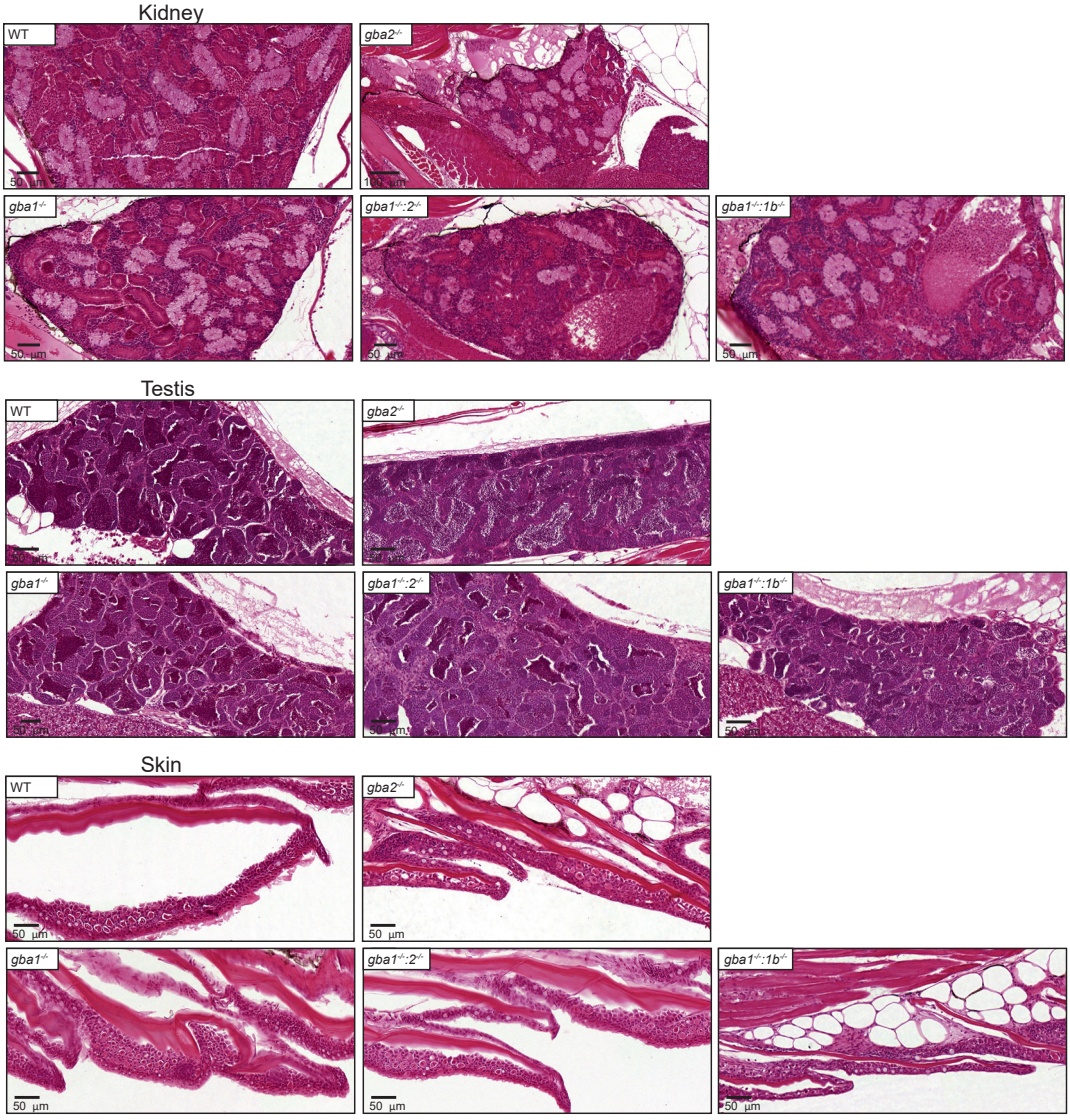

Supplementary Figure 2 | H&E staining of kidney, testis and skin of WT and mutant zebrafish.

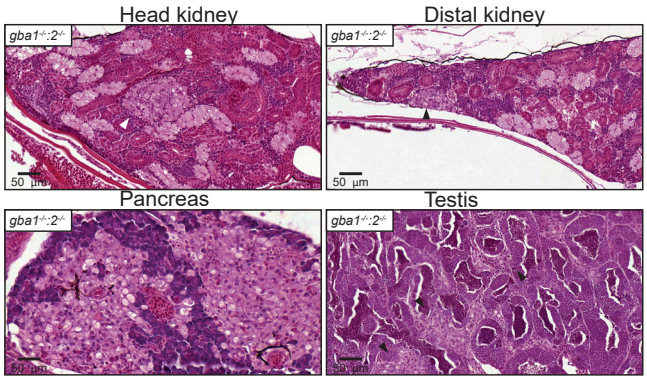

Supplementary Figure 3 | H&E staining of one individual, severe *gba1*$^{-/-}$:gba2$^{-/-}$ zebrafish head kidney, distal kidney and testis. Patches with Gaucher-like cells are marked with arrows.

Supplementary Figure 4 | Different gba1$^{-/-}$ and gba1$^{-/-}$:gba2$^{-/-}$ zebrafish at 10, 11 and 12 wpf as well as WT and *gba1*$^{-/-}$*:asah1b*$^{-/-}$ individuals at 12 wpf.

Supplementary Table 1 | Overview of findings in brains of WT, *gba1*$^{+/-}$ carriers, *gba1*, gba2, *gba1:gba2*, *asah1b* and *gba1:asah1b* KO fish.

	Lipids			mRNA expression				Pathology
Enzyme	**GlcSph**	**GlcCer**	**GlcChol**	**Storage cells**	**Inflammation**	**Complement activation**	**th & synucleins**	**Infiltration of Gaucher-like cells**
WT	-	-	-	-	-	-	-	-
gba1$^{+/-}$	-	-	-	-	-	-	-	-
gba1 KO	↑↑	↑↑ Only 18:0	↑	↑↑	↑	↑	↓	↑
gba2 KO	-	-	-	-	-	-	-	-
gba1:gba2 KO	↑↑	↑↑↑	-	↑↑	↑	↑	↓	↑
asah1b KO	-	-	-	-	-	-	-	-
asah1b:gba1 KO	-	↑↑	-	↑↑	↑	↑	-	↑

Experimental procedures

Chemicals and reagents - GCase specific inhibitor (ME656)[44], $^{13}C_5$-sphinganine, $^{13}C_5$-sphingosine, $^{13}C_5$-GlcSph, $^{13}C_5$-lyso-globotriaosylceramide (LysoGb3), C17-lysosphingo-myelin (LysoSM), $^{13}C_6$-GlcChol and C17-dihydroceramide (dhCer)[25,30] were synthesized as reported. All chemicals and reagents were obtained from Sigma-Aldrich Chemie Gmbh (St Louis, USA) unless mentioned otherwise. The standards Cer (d18:1/16:0), dhCer (d18:0/16:0), GlcCer (d18:1/16:0), GalCer (d18:1/16:0), LacCer (d18:1/16:0) were obtained from Avanti Polar lipids (Alabaster, USA) and GlcChol from Sigma-Aldrich. LC-MS grade methanol, 2-propanol, water, formic acid, acetonitrile and HPLC grade chloroform were purchased from Biosolve (Valkenswaard, the Netherlands). LC-MS grade ammonium formate, ammonium acetate and sodium hydroxide from Sigma-Aldrich, butanol and hydrochloric acid from Merck Millipore (Billerica, USA).

Zebrafish - All zebrafish were housed and maintained at the University of Leiden, the Netherlands, according to standard protocols. Wildtype (WT) zebrafish (ABTL) were a mixed lineage of WT AB and WT TL genetic backgrounds. Zebrafish were kept at constant temperature of 28.5 °C and on a cycle of 14-hour light and 10 hour dark. CRISPR/Cas9 mediated knockout zebrafish of *gba1, gba2* and *asah1b* were generated and maintained as described in chapters 4, 5 and 6. Heterozygous (*gba1* background) or homozygous (*gba2* or *asah1b* background) adults were in-crossed and raised to adulthood (*gba2*$^{-/-}$) or genotyped at 4-5 dpf before raising to adulthood (*gba1*$^{+/-}$, *gba1*$^{-/-}$, *gba1*$^{-/-}$*:gba2*$^{-/-}$, *asah1b*$^{-/-}$ and *gba1*$^{-/-}$*:asah1b*$^{-/-}$). Experiments with larvae, juvenile and adult zebrafish after the free-feeding stage were approved by the local animal welfare committee (Instantie voor Dierwelzijn) of the University Leiden (Project license AVD1060020184725). Zebrafish from 5 dpf to 2 wpf were fed with both dry food (2x daily; Skretting Gemma micro 75, Zebcare, Nederweert, the Netherlands) and Rotifers (1x daily) and from 3 wpf to the end of the experiment fed with both dry food (2x daily; Skretting Gemma micro 150 until 30 dpf or Gemma Micro 300 mixed with Gemma Diamond for fish from 30 dpf) and hatched Artemia (1x daily).

Zebrafish sampling – Zebrafish were sacrificed at 12 wpf or earlier when zebrafish showed symptoms noted as human endpoints. From 8 wpf, zebrafish were monitored extensively for phenotypic and morphological symptoms such as curvature of the back and abnormal swimming behaviour. Human endpoints were defined as follows: 1) fish having a moderate to extreme curvature of the spine independent of the feeding consumption, 2) fish with a slight curvature but clear abnormal swimming behaviour or 3) fish with a slight curvature which are unable to reach and consume the provided food. *Gba1*$^{-/-}$ zebrafish were sacrificed between 10 and 12 wpf, while no symptoms were observed for WT, *asah1b*$^{-/-}$ and *gba1*$^{-/-}$*:asah1b*$^{-/-}$. The same human endpoints were used for the longevity study of the *gba1*$^{-/-}$*:asah1b*$^{-/-}$. Individual zebrafish were transferred to single tanks (1 L external breeding tank with lid, Techniplast, West Chester, USA) acclimatized for 10 minutes and recorded as described below. Afterwards, fish were sacrificed using an overdose of tricaine methane sulfonate (MS222, 200 mg/L) and photographed using a Leica M165C microscope (Wetzlar, Germany). Whole zebrafish were fixed for histopathology or organs were dissected. Dissected organs were either snap frozen in liquid nitrogen for protein and (glyco)sphingolipid analysis or submerged in RNAlater (Invitrogen, Thermo Fisher Scientific, Waltham USA) for RT-PCR analysis (brain or liver) and stored at -80 °C.

Movement analysis – The individual tanks were randomly placed in a 3x4 or 4x4 setup and the camera was placed at a distance dependent on the setup to include all tanks. Zebrafish were left for at least 10 min to acclimatize and recorded for 20 min using a Sony A6000 camera (Tokyo, Japan) with a 30 mm objective. Movements of the fish in the individual tank were tracked using Ethiovision software 10.1 (Noldus, Wageningen, the Netherlands). Arenas were setup for each individual tank by drawing a rectangular shape in the tank, thereby not including any reflections at the top, bottom and sides. The arenas without reflection accompanied approximately 46 ± 5% of the total area of the individual tank (± 17 cm length x 8 cm weight). A horizontal and vertical line were used to calibrate the area

to the measurements of the tank and each arena was divided in two equal zones: a top and bottom zone. The detection settings were set as follows: model-based and differencing settings for Nose-tail detection; the subject colour was brighter than background, sensitivity of 45; subject size with a minimum of 80 and maximum of 2042 pixels and video sample rate of 6.25 per sec. Data was acquired every 0.16 sec for a total of 10 minutes after a 5 min delay. The data was exported and the velocity was calculated by averaging the velocity of all datapoints, while the time spend in the bottom zone was obtained by dividing the amount time spend in the bottom zone by the total time.

Zebrafish morphology – The three or four images of one fish, obtained with the Leica microscope, were stitched to obtain one image using Photoshop CC2018 (Adobe, San Jose, USA) The length of the fish from head to tail base (body length) was determined as well as the length of the back from head to tail base (long length) using ImageJ software. The tortuosity was calculated by dividing the long length by the body length.

Homogenate preparation - Homogenates of organs were prepared in potassium phosphate (KPi lysis buffer; 25 mM K_2HPO_4-KH_2PO_4 pH 6.5, 0.1% (v/v) Triton-X100 and EDTA-free protease inhibitor (cOmplete™, EDTA-free Protease Inhibitor Cocktail, Roche, Sigma-Aldrich). Organs were first homogenized using a Dounce homogenizer (10 strokes) followed by sonication (20% amplitude, 3 sec on, 3 sec off for 4 cycles) using a Vibra-Cell VCX 130 (Sonics, Newtown, USA) while on ice. Total protein concentration of homogenates was determined using Pierce BCA protein assay kit (Thermo Fisher Scientific, Waltham, USA) and measured using an EMax® plus microplate reader (Molecular Devices, Sunnyvale, USA).

Western blot - Proteins of organ homogenates (20 µg protein) were denatured using 5x Laemmli sample buffer (25% (v/v) 1.25M Tris-HCL pH 6.8, 50% (v/v) 100% glycerol, 10% (w/v) sodium dodecyl sulphate (SDS), 8% (w/v) dithiothreitol (DTT) and 0.1% (w/v) bromophenol blue), samples were boiled for 5 min at 98 °C and proteins were separated by electrophoresis on a 12% (w/v) SDS-PAGE gel. Proteins were transferred to nitrocellulose membranes (0.2 µM, Bio-Rad laboratories Inc., Hercules, USA) using the Trans-Blot® Turbo™ Transfer system (Bio-Rad). Membranes were blocked with 5% (w/v) bovine albumin serum (BSA) and incubated overnight at 4 °C with primary antibodies: rabbit anti-LC3 (1:1000, NB100-2220; Novus Biologicals, Centennial, USA), rabbit anti-p62/SQSTM1 (1:1000, P0067; Sigma) or rabbit anti-actin (1:1000, ab209857; Abcam, Cambridge, UK). Membranes were washed 3 times with TBST and incubated for 1 h at RT with secondary antibody: GARPO goat anti rabbit IgG (H+L) peroxidase (1:5000, Bio-Rad). Chemiluminescence signal is developed using the Clarity Max Western ECL substrate (Bio-Rad), detected using a ChemiDocMP imager (Bio-Rad) and signal quantified by ImageJ software.

Gene expression analysis - RNAlater was removed and RNA was extracted using a Nucleospin RNA XS column (Machinery-Nagel, Düren, Germany) procedure according to suppliers protocol, without the addition of carrier RNA. Contaminating DNA was degraded on column by a DNase I treatment (supplied in the kit). cDNA was synthesized using SuperScript II reverse transcriptase (Invitrogen, ThermoFisher Scientific, Waltham, USA) using oligo(dT) and an input of approximately 200-500 ng total RNA according to the manufacturer's instruction. Generated cDNA was diluted to an approximate concentration of 0.5 ng total RNA input/µL with Milli-Q water. QPCR reactions were performed with the IQ SYBR green mastermix (Bio-Rad laboratories Inc., Hercules, USA) in a total volume of 15 µL (1x SYBR green, 333 µM of forward and reverse primer as given in Supplementary Table 2 and 5 µL of the diluted cDNA input) and carried out using a CFX96™ Real-Time PCR Detection system (Bio-Rad laboratories Inc., Hercules, USA) with the following conditions: denaturation at 95 °C for 3 min, followed by 40 cycles of amplification (95 °C for 30 sec and 61 °C for 30 sec), imaging the plate after every extension at 61 °C, followed by a melt program from 55-95 °C with 0.5 °C per step with imaging the plate every step. All biological samples were tested in technical duplicate, differential gene expression was calculated using the ΔΔCτ method normalized to two house-keeping genes *ef1a* and *rpl13* and depicted as $\log_2$ fold change ± SEM, compared to WT.

Supplementary Table 2| Forward and reverse primers for RT-qPCR analysis.

Target	NCBI code	Forward primer sequence (5'->3')	Reverse primer sequence (5'->3')	
Asah1a	NM_001006088	ATTAGGCCTGGTGAACTGAC	CTGCGAGTAAGAAAACCCGTC	125 bp
Asah1b	NM_200577	TGGACTGTTCATGGGATGGG	CCGGTCAACATCCCGACATA	150 bp
Gpnmb	XM_009294247	GCAAGGGCGTAGAATTGAAA	TGGCAGGGACATGTCAGTAA	
Chia.6	NM_199603	TCCACGGCTCATGGGAGAGTGTC	AGCGCCCTGATCTCGCCAGT	ref. 45
catD	NM_131710	TGGGTGGAAAGGTCTACTCG	CACTCAGGCAGATGTCGTGT	
il1ß	NM_212844	TGGACTTCGCAGCACAAAATG	GTTCACTTCACGCTCTTGGATG	ref. 46
tnfß	NM_182873	GCATGTGATGAAGCCAAACG	GATTGTCCTGAAGGGTCACC	ref. 47
apoeb	NM_131098	AAACTGACATGACCGACGCT	TAGGTTGCTACGGTGTTGCG	172 bp
c1qA	NM_001020527	CTCTGTTTCCCTTTTCCTTCTG	CTTTCTCTCCTTTTGGTCCTGG	108 bp
c3a.1	NM_131242	CGCTGCACAAAGTACTTCCAC	GCCAGCTCCATGTCCTTGAC	197 bp
c5aR1	XM_005159274	CCGACAAGCTCGCATCCTAT	GCGAATGATGGTTATCGCCC	163 bp
c5	XM_001919191	CAAGGCCACGGTTCAATCAG	TCTTCATGCTTTCGGCAGTCA	152 bp
th1	NM_131149	AGCTTTGTGGACGCTACTGA	GTGGGTTGTCCAGCACTTCT	112 bp
th2	NM_001001829	TACAAGCCATTCGACCCAGC	ATGCTGCAAGTGTAGGGGTC	173 bp
sncß	NM_200969	GGAGTTTGGTCAGGAAGCCA	CCTCGGGCTCATAATCCTGG	107 bp
sncγa	NM_001017567	TGGAGGGGCTGGAGACTATG	AGCATCATGGGACATTCGGTT	123 bp
sncγb	NM_001020652	ATGGTGAACCCGGGTGACTT	AGGCTTTGGAGCAGAAACGTA	129 bp
mcpa	XM_002665562	TGGTCATCTATCCTCCTCTCCA	CTTTCTCCCAGGCCCAATAGTTCT	150 bp
ef1a		CTGGAGGCCAGCTCAAACAT	ATCAAGAAGAGTAGTACCGCTAGCATTAC	ref. 48
rpl13α		TCTGGAGGACTGTAAGAGGTATGC	AGACGCACAATCTTGAGAGCAG	ref. 48

(Glyco)sphingolipid (GSL) analysis - Neutral (glyco)lipids, (glyco)sphingoid bases and glycosylated cholesterol were extracted from the same homogenate (10 µL, 20-30 µg total protein in KPi lysis buffer) using an acidic Bligh and Dyer procedure (1/1/0.9 chloroform/methanol/100 mM formate buffer pH 3.1) as described before[27,30]. Lipids were resuspended in acetonitrile/methanol (9/1, v/v) for separation using a HILIC column and transferred to a vial for LC-MS/MS analysis. LC-MS/MS measurements were performed using a Waters UPLC-Xevo-TQS micro instrument (Waters, Corporation, Milford, USA) in positive mode using an electrospray ionization (ESI) with a BEH HILIC column (2.1 x 100 mm with 1.7 µm particle size, Waters) was used at 30 °C as described before[27] with minor modifications in the eluent program allowing a faster run while preserving separation of Glc- and Gal containing lipids. Eluent A contained 10 mM ammonium formate in acetonitrile/water (97:3, v/v) with 0.01% (v/v) formic acid and eluent B consisted of 10 mM ammonium formate in acetonitrile/water (75:15, v/v) with 0.01% (v/v) formic acid. Lyso- and deacylated glycosphingolipids were eluted in 10 min with a flow of 0.6 mL/min using the following program: 85% A from 0-1 min, 85-65% A from 1-2.5 min, 60-0% A from 2.5-4 min, 0% A from 4-4.5, 0-85% A from 4.5-4.6 min and re-equilibration with 85% A from 4.6-10 min. GlcChol was eluted in 18 min with a flow of 0.25 ml/min using the following program: 100% A from 0-3 min, 100-0 % A from 3-3.5 min, 0 % A from 3.5-4.5 min, 0-100

% A from 4.5-5 min and re-equilibration with 100 % A from 5-18 min. Lipid levels were calculated in pmol/mg total protein, sphingoid bases and GlcChol were calculated based on the respective isotopic ^{13}C internal standard, while deacylated neutral (glyco)sphingolipids were calculated using C17-dhCer as internal standard and normalized using the respective standard.

For the analysis of neutral glycosphingolipids with fatty acyls, 20 µL of the intenal standard dhCer d17:0/16:0 (20 pmol/µL in methanol) and 20 µL of SM d18:1/17:0 (20 pmol/µL in methanol) was added to homogenates (10 µL, ± 10 µg total protein in KPi lysis buffer) and lipids were extracted using an acidic Bligh and Dyer procedure (1/1/0.9 chloroform/methanol/100 mM formate buffer pH 3.1), the lower phase was collected, dried and a butanol/water extraction was performed. Lipids were resuspended in acetonitrile/methanol (9/1, v/v) for separation using a HILIC column and transferred to a vial for LC-MS/MS analysis. The same eluent composition was used as described above and neutral glycosphingolipids were eluted in 23 min with a flow of 0.25 mL/min using the following program: 100% A from 0-3 min, 100-70% A from 3.-3.5 min, 70% A from 3.5-6 min, 70-0% A from 6-9.5 min, 0% A from 9.5-10.5 min and re-equilibration with 100% A from 10.6-23 min. Lipid levels were calculated based on SM d18:1/16:0 for SM lipids or dhCer d17:0/16:0 for the other glycosphingolipids, normalized using the protein concentration and depicted as ratio compared WT.

Supplementary Table 3| Tansitions, cone voltage and collision energy of neutral GSLs with different fatty acyls.

Lipid	Transition	Cone	Collission	Lipid	Transition	Cone	Collission
dhCer d17:0/16:0 (IS)	526.7>264.4	10	20				
Cer d18:1/16:1	536.6>264.4	10	20	HexCer d18:1/16:1	698.6>264.4	10	44
Cer d18:1/16:0	538.6>264.4	10	20	HexCer d18:1/16:0	700.6>264.4	10	44
Cer d18:1/18:1	564.6>264.4	10	20	HexCer d18:1/18:1	726.6>264.4	10	44
Cer d18:1/18:0	566.6>264.4	10	20	HexCer d18:1/18:0	728.6>264.4	10	44
Cer d18:1/20:1	592.6>264.4	10	20	HexCer d18:1/20:1	754.6>264.4	10	46
Cer d18:1/20:0	594.6>264.4	10	20	HexCer d18:1/20:0	756.6>264.4	10	46
Cer d18:1/22:1	620.6>264.4	10	20	HexCer d18:1/22:1	782.6>264.4	10	48
Cer d18:1/22:0	622.6>264.4	10	20	HexCer d18:1/22:0	784.6>264.4	10	48
Cer d18:1/24:1	648.6>264.4	10	20	HexCer d18:1/24:1	810.6>264.4	10	52
Cer d18:1/24:0	650.6>264.4	10	20	HexCer d18:1/24:0	812.6>264.4	10	52
SM d18:1/17:0 (IS)	717.6>264.4	30	30				
SM d18:1/16:1	701.6>184.1	30	30				
SM d18:1/16:0	703.6>184.1	30	30	LacCer d18:1/16:0	862.7>264.4	30	48
SM d18:1/18:1	729.6>184.1	30	30				
SM d18:1/18:0	731.6>184.1	30	30	LacCer d18:1/18:0	890.7>264.4	30	48
SM d18:1/20:1	757.6>184.1	30	30				
SM d18:1/20:0	759.6>184.1	30	30				
SM d18:1/22:1	785.7>184.1	30	30				
SM d18:1/22:0	787.7>184.1	30	30				
SM d18:1/24:1	813.7>184.1	30	40	LacCer d18:1/24:1	972.8>264.4	30	50
SM d18:1/24:0	815.7>184.1	30	40	LacCer d18:1/24:0	974.8>264.4	30	50

Histology - For H&E staining, zebrafish were fixed in paraformaldehyde (4% PFA (w/v), Alfa Aesar, Haverhill, USA) overnight or Bouin's solution (5% acetic acid, 9% formaldehyde, 0.9% picric acid, Sigma) for 4 days, decalcified for 4 days using formic acid (20% (v/v)) and embedded in paraffin. Subsequently, serial sections of 5 µM thickness were made using a Leica RM2055 microtome. Sections were stained with Haematoxylin and Eosin.

Statistical analyses - Statistical analyses were performed using GraphPad Prism (v8.1.1, GraphPadsoftware, CA, USA) and data depicted as described in the result section. Data of lipid, protein and mRNA levels was analysed by One-Way Anova using Dunnett's test, with WT as control group, or Tukey's multiple comparison test as described in the result section. Data of length and tortuosity are analysed using a non-parametric Kruskal-Wallis test with Dunn's multiple comparison. In general, statistical comparisons are performed of WT vs *gba1*$^{-/-}$, WT vs *gba1*$^{-/-}$*:asah1b*$^{-/-}$ and *gba1*$^{-/-}$ vs *gba1*$^{-/-}$*:asah1b*$^{-/-}$, and depicted only when a significant difference is apparent and relevant. Ns = not significant, * $P< 0.05$, ** $P< 0.01$, *** $P< 0.001$ and **** $P< 0.0001$.

References

1. Brady R.O., Kanfer J.N., Bradley R.M.and Shapiro D. (1966) Demonstration of a deficiency of glucocerebroside-cleaving enzyme in Gaucher's disease. *The Journal of clinical investigation* **45**, 1112-1115.
2. Nair S., Boddupalli C.S., Verma R., Liu J., Yang R., Pastores G.M.,... and Dhodapkar M.V. (2015) Type II NKT-TFH cells against Gaucher lipids regulate B-cell immunity and inflammation. *Blood* **125**, 1256-1271.
3. Ikuno M., Yamakado H., Akiyama H., Parajuli L.K., Taguchi K., Hara J.,... and Takahashi R. (2019) GBA haploinsufficiency accelerates alpha-synuclein pathology with altered lipid metabolism in a prodromal model of Parkinson's disease. *Human molecular genetics* **28**, 1894-1904.
4. Taguchi Y.V., Liu J., Ruan J., Pacheco J., Zhang X.,... and Chandra S.S. (2017) Glucosylsphingosine Promotes alpha-Synuclein Pathology in Mutant GBA-Associated Parkinson's Disease. *J Neurosci* **37**, 9617-9631.
5. Smith N.J., Fuller M., Saville J.T.and Cox T.M. (2018) Reduced cerebral vascularization in experimental neuronopathic Gaucher disease. *J Pathol* **244**, 120-128.
6. Sidransky E., Nalls M.A., Aasly J.O., Aharon-Peretz J., Annesi G., Barbosa E.R.,... and Ziegler S.G. (2009) Multicenter analysis of glucocerebrosidase mutations in Parkinson's disease. *New England Journal of Medicine* **361**, 1651-1661.
7. Tsuang D., Leverenz J.B., Lopez O.L., Hamilton R.L., Bennett D.A., Schneider J.A.,... and Zabetian C.P. (2012) GBA mutations increase risk for Lewy body disease with and without Alzheimer disease pathology. *Neurology* **79**, 1944-1950.
8. Hammer M.B., Eleuch-Fayache G., Schottlaender L.V., Nehdi H., Gibbs J.R., ... and Singleton A.B. (2013) Mutations in GBA2 cause autosomal-recessive cerebellar ataxia with spasticity. *Am J Hum Genet* **92**, 245-251.
9. Woeste M.A.and Wachten D. (2017) The Enigmatic Role of GBA2 in Controlling Locomotor Function. *Front Mol Neurosci* **10**, 386.
10. Martin E., Schule R., Smets K., Rastetter A., Boukhris A., Loureiro J.L.,... and Stevanin G. (2013) Loss of function of glucocerebrosidase GBA2 is responsible for motor neuron defects in hereditary spastic paraplegia. *Am J Hum Genet* **92**, 238-244.
11. Votsi C., Zamba-Papanicolaou E., Middleton L.T., Pantzaris M.and Christodoulou K. (2014) A novel GBA2 gene missense mutation in spastic ataxia. *Ann Hum Genet* **78**, 13-22.
12. Overkleeft H.S., Renkema G.H., Neele J., Vianello P., Hung I.O.,... and Aerts J.M. (1998) Generation of specific deoxynojirimycin-type inhibitors of the non-lysosomal glucosylceramidase. *J Biol Chem* **273**, 26522-26527.
13. Giraldo P., Andrade-Campos M., Alfonso P., Irun P., Atutxa K., Acedo A.,... and Pocovi M. (2018) Twelve years of experience with miglustat in the treatment of type 1 Gaucher disease: The Spanish ZAGAL project. *Blood Cells Mol Dis* **68**, 173-179.
14. Farfel-Becker T., Vitner E.B.and Futerman A.H. (2011) Animal models for Gaucher disease research. *Dis Model Mech* **4**, 746-752.
15. Sidransky E., Sherer D.M.and Ginns E.I. (1992) Gaucher disease in the neonate: a distinct Gaucher phenotype is analogous to a mouse model created by targeted disruption of the glucocerebrosidase gene. *Pediatr Res* **32**, 494-498.
16. Tybulewicz V.L., Tremblay M.L., LaMarca M.E., Willemsen R., Stubblefield B.K., Winfield S.,... and et al. (1992) Animal model of Gaucher's disease from targeted disruption of the mouse glucocerebrosidase gene. *Nature* **357**, 407-410.
17. Vardi A., Zigdon H., Meshcheriakova A., Klein A.D., Yaacobi C., Eilam R.,... and Futerman A.H. (2016) Delineating pathological pathways in a chemically induced mouse model of Gaucher disease. *J Pathol* **239**, 496-509.
18. Mistry P.K., Liu J., Yang M., Nottoli T., McGrath J., Jain D.,... and Zaidi M. (2010) Glucocerebrosidase gene-deficient mouse recapitulates Gaucher disease displaying cellular and molecular dysregulation beyond the macrophage. *Proc Natl Acad Sci U S A* **107**, 19473-19478.
19. Enquist I.B., Lo Bianco C., Ooka A., Nilsson E., Mansson J.E., Ehinger M.,... and Karlsson S. (2007) Murine models of acute neuronopathic Gaucher disease. *Proc Natl Acad Sci U S A* **104**, 17483-17488.
20. Yildiz Y., Matern H., Thompson B., Allegood J.C., Warren R.L., Ramirez D.M.,... and Russell D.W. (2006) Mutation of beta-glucosidase 2 causes glycolipid storage disease and impaired male fertility. *The Journal of clinical investigation* **116**, 2985-2994.
21. Woeste M.A., Stern S., Raju D.N., Grahn E., Dittmann D., Gutbrod K.,... and Wachten D. (2019) Species-specific differences in nonlysosomal glucosylceramidase GBA2 function underlie locomotor dysfunction arising from loss-of-function mutations. *J Biol Chem* **294**, 3853-3871.
22. Raju D., Schonauer S., Hamzeh H., Flynn K.C., Bradke F.,... and Wachten D. (2015) Accumulation of glucosylceramide in the absence of the beta-glucosidase GBA2 alters cytoskeletal dynamics. *Plos Genet* **11**, e1005063.
23. Mistry P.K., Liu J., Sun L., Chuang W.L., Yuen T., Yang R.,... and Zaidi M. (2014) Glucocerebrosidase 2 gene deletion rescues type 1 Gaucher disease. *Proc Natl Acad Sci U S A* **111**, 4934-4939.
24. Marques A.R., Aten J., Ottenhoff R., van Roomen C.P., Herrera Moro D., Claessen N.,... and Aerts J.M. (2015)

Reducing GBA2 Activity Ameliorates Neuropathology in Niemann-Pick Type C Mice. *PloS one* **10**, e0135889.
25. Marques A.R., Mirzaian M., Akiyama H., Wisse P., Ferraz M.J., Gaspar P.,... and Aerts J.M. (2016) Glucosylated cholesterol in mammalian cells and tissues: formation and degradation by multiple cellular beta-glucosidases. *J Lipid Res* **57**, 451-463.
26. Akiyama H.and Hirabayashi Y. (2017) A novel function for glucocerebrosidase as a regulator of sterylglucoside metabolism. *Biochim Biophys Acta Gen Subj* **1861**, 2507-2514.
27. Lelieveld L.T., Mirzaian M., Kuo C.L., Artola M., Ferraz M.J., Peter R.E.A.,... and Aerts J. (2019) Role of beta-glucosidase 2 in aberrant glycosphingolipid metabolism: model of glucocerebrosidase deficiency in zebrafish. *J Lipid Res* **60**, 1851-1867.
28. Akiyama H., Ide M., Nagatsuka Y., Sayano T., Nakanishi E., Uemura N.,... and Hirabayashi Y. (2020) Glucocerebrosidases catalyze a transgalactosylation reaction that yields a newly-identified brain sterol metabolite, galactosylated cholesterol. *J Biol Chem* **295**, 5257-5277.
29. Groener J.E., Poorthuis B.J., Kuiper S., Helmond M.T., Hollak C.E.and Aerts J.M. (2007) HPLC for simultaneous quantification of total ceramide, glucosylceramide, and ceramide trihexoside concentrations in plasma. *Clin Chem* **53**, 742-747.
30. Mirzaian M., Wisse P., Ferraz M.J., Marques A.R.A., Gaspar P., Oussoren S.V.,... and Aerts J.M. (2017) Simultaneous quantitation of sphingoid bases by UPLC-ESI-MS/MS with identical (13)C-encoded internal standards. *Clin Chim Acta* **466**, 178-184.
31. Sugawara T.and Miyazawa T. (1999) Separation and determination of glycolipids from edible plant sources by high-performance liquid chromatography and evaporative light-scattering detection. *Lipids* **34**, 1231-1237.
32. Nystrom L., Schar A.and Lampi A.M. (2012) Steryl glycosides and acylated steryl glycosides in plant foods reflect unique sterol patterns. *Eur J Lipid Sci Tech* **114**, 656-669.
33. Lawrence C. (2011) Advances in zebrafish husbandry and management. *Methods Cell Biol* **104**, 429-451.
34. Spence R., Gerlach G., Lawrence C.and Smith C. (2008) The behaviour and ecology of the zebrafish, Danio rerio. *Biological reviews of the Cambridge Philosophical Society* **83**, 13-34.
35. Farfel-Becker T., Vitner E.B., Kelly S.L., Bame J.R., Duan J., Shinder V.,... and Futerman A.H. (2014) Neuronal accumulation of glucosylceramide in a mouse model of neuronopathic Gaucher disease leads to neurodegeneration. *Human molecular genetics* **23**, 843-854.
36. Farfel-Becker T., Vitner E.B., Pressey S.N., Eilam R., Cooper J.D.and Futerman A.H. (2011) Spatial and temporal correlation between neuron loss and neuroinflammation in a mouse model of neuronopathic Gaucher disease. *Human molecular genetics* **20**, 1375-1386.
37. Vitner E.B., Farfel-Becker T., Eilam R., Biton I.and Futerman A.H. (2012) Contribution of brain inflammation to neuronal cell death in neuronopathic forms of Gaucher's disease. *Brain* **135**, 1724-1735.
38. Zigdon H., Savidor A., Levin Y., Meshcheriakova A., Schiffmann R.and Futerman A.H. (2015) Identification of a biomarker in cerebrospinal fluid for neuronopathic forms of Gaucher disease. *PloS one* **10**, e0120194.
39. Klein A.D., Ferreira N.S., Ben-Dor S., Duan J., Hardy J., Cox T.M.,... and Futerman A.H. (2016) Identification of Modifier Genes in a Mouse Model of Gaucher Disease. *Cell Rep* **16**, 2546-2553.
40. Jones E.E., Zhang W., Zhao X., Quiason C., Dale S., Shahidi-Latham S.,... and Sun Y. (2017) Tissue Localization of Glycosphingolipid Accumulation in a Gaucher Disease Mouse Brain by LC-ESI-MS/MS and High-Resolution MALDI Imaging Mass Spectrometry. *SLAS Discov* **22**, 1218-1228.
41. Keatinge M., Bui H., Menke A., Chen Y.C.,... and Bandmann O. (2015) Glucocerebrosidase 1 deficient Danio rerio mirror key pathological aspects of human Gaucher disease and provide evidence of early microglial activation preceding alpha-synuclein-independent neuronal cell death. *Human molecular genetics* **24**, 6640-6652.
42. Blesa J., Trigo-Damas I., Quiroga-Varela A.and Jackson-Lewis V.R. (2015) Oxidative stress and Parkinson's disease. *Front Neuroanat* **9**, 91.
43. Pandey M.K., Burrow T.A., Rani R., Martin L.J., Witte D., Setchell K.D.,... and Grabowski G.A. (2017) Complement drives glucosylceramide accumulation and tissue inflammation in Gaucher disease. *Nature* **543**, 108-112.
44. Artola M., Kuo C.L., Lelieveld L.T., Rowland R.J., van der Marel G.A., Codee J.D.C.,... and Overkleeft H.S. (2019) Functionalized Cyclophellitols Are Selective Glucocerebrosidase Inhibitors and Induce a Bona Fide Neuropathic Gaucher Model in Zebrafish. *Journal of the American Chemical Society* **141**, 4214-4218.
45. Koch B.E., Stougaard J.and Spaink H.P. (2014) Spatial and temporal expression patterns of chitinase genes in developing zebrafish embryos. *Gene Expr Patterns* **14**, 69-77.
46. Nguyen-Chi M., Laplace-Builhe B., Travnickova J., Luz-Crawford P., Tejedor G., Lutfalla G.,... and Djouad F. (2017) TNF signaling and macrophages govern fin regeneration in zebrafish larvae. *Cell Death Dis* **8**, e2979.
47. Harjula S.E., Ojanen M.J.T., Taavitsainen S., Nykter M.and Ramet M. (2018) Interleukin 10 mutant zebrafish have an enhanced interferon gamma response and improved survival against a Mycobacterium marinum infection. *Sci Rep* **8**, 10360.
48. Tang R., Dodd A., Lai D., McNabb W.C.and Love D.R. (2007) Validation of zebrafish (Danio rerio) reference genes for quantitative real-time RT-PCR normalization. *Acta Biochim Biophys Sin (Shanghai)* **39**, 384-390